UCRL-93926
PREPRINT

ATOMS IN DENSE PLASMAS

Richard M. More

Lawrence Livermore National Laboratory
University of California
Livermore, CA 94550

This paper was prepared for the
NATO Advanced Study Institute
"Atoms in Unusual Situations"
Institut d'Etudes Scientifiques de Cargese
Cargese, Corsica

January 1986

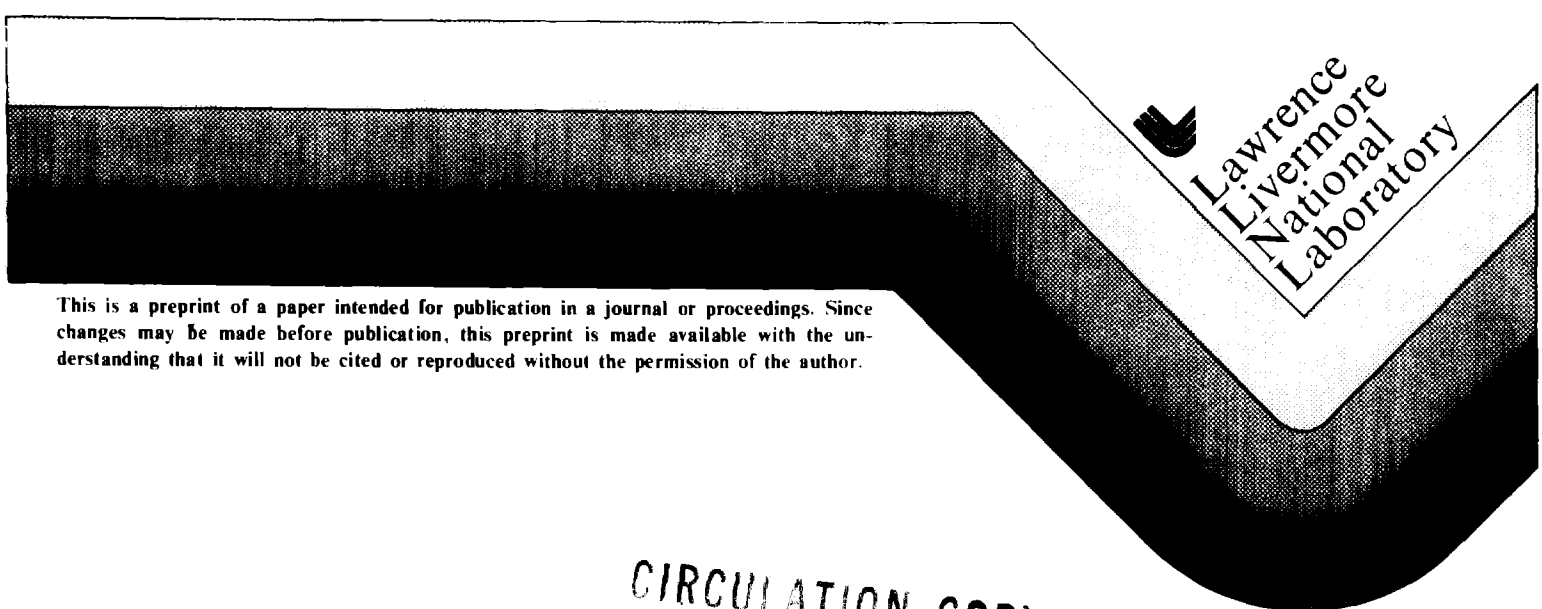

ABSTRACT

Recent experiments with high-power pulsed lasers have strongly encouraged the development of improved theoretical understanding of highly charged ions in a dense plasma environment. This work examines the theory of dense plasmas with emphasis on general rules which govern matter at extreme high temperature and density.

ATOMS IN DENSE PLASMAS

Richard M. More

Lawrence Livermore National Laboratory
University of California
Livermore, CA 94550

When laser light is focussed to intensities of 10^{14} - 10^{16} Watt/cm^2 onto a cold solid, the target surface promptly rises to temperatures ~0.1 - 1 keV and produces a highly ionized plasma. Heat energy absorbed from the laser penetrates into the cold target by nonlinear electron heat conduction driven by enormous temperature gradients (~ 10^9 °K/cm), large thermoelectric and magnetic fields are generated, thermally produced x-rays are emitted and the heated material expands in high-velocity hydrodynamic flow. For all these processes the working fluid is a dense plasma of highly-charged ions. Because the densities and/or temperatures greatly exceed those available in previous laboratory plasma devices, we find many interesting new topics for scientific investigation.[1,2,3,4]

This paper covers some aspects of the theory of atomic processes in dense plasmas. Because the topic is very broad, we have selected a few general rules which give useful guidance about the typical behavior of dense plasmas. These rules are illustrated by semiclassical estimates, scaling laws and appeals to more elaborate calculations.

Included in the paper are several previously unpublished results including a new mechanism for electron-ion heat exchange (section II), and an approximate expression for oscillator-strengths of highly charged ions (section V). However the main emphasis is not upon practical formulas but rather on questions of fundamental theory, the structural ingredients which must be used in building a model for plasma events. What are the density effects and how does one represent them? Which are most important? How does one identify an incorrect theory? The general rules help to answer these questions.

Unfortunately in most cases one cannot yet directly employ experimental data to resolve theoretical questions. This circumstance has been, for many years, a basic difficulty of research on dense plasmas. For example, in

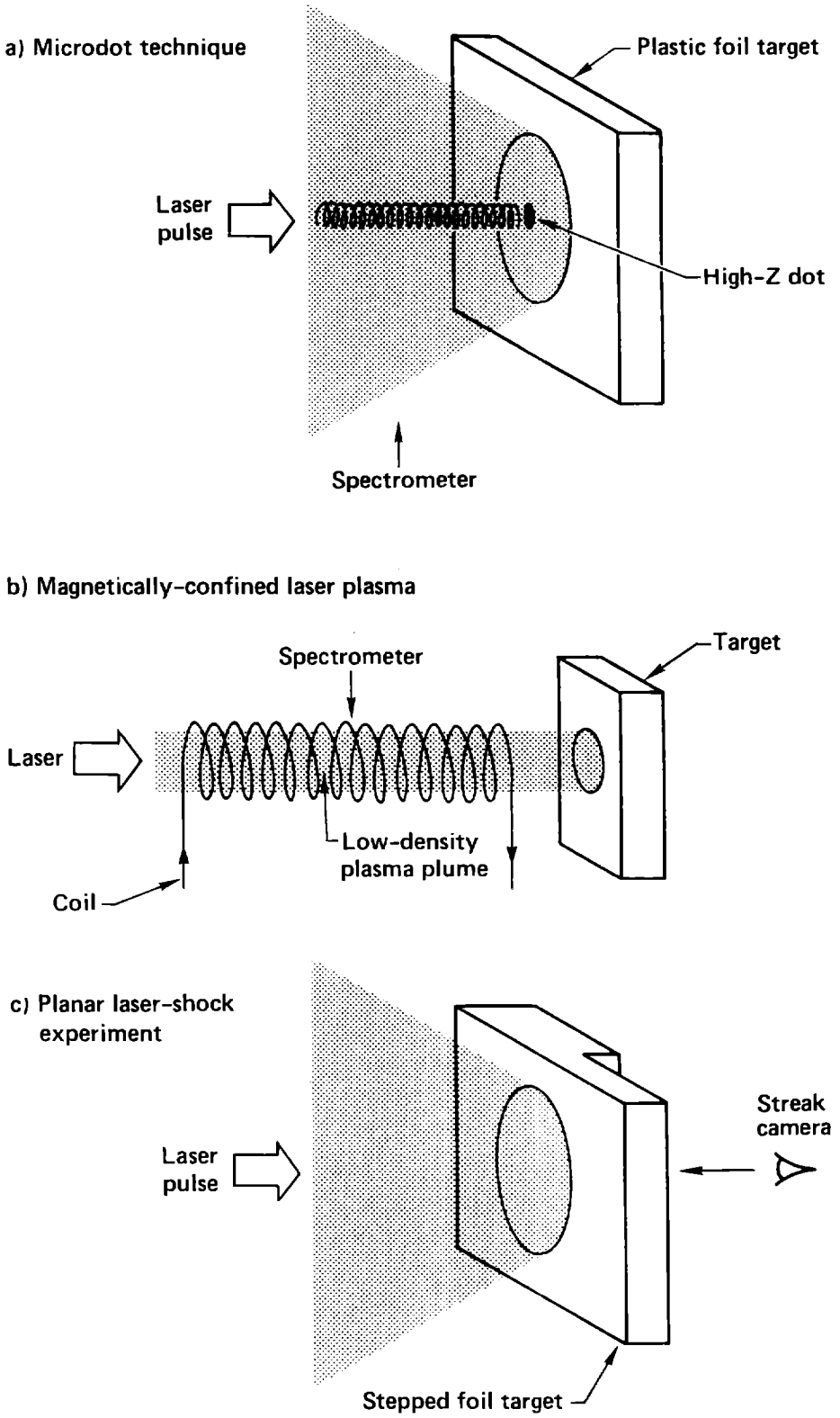

FIG. 1. Three favorable geometries for scientific experiments in laser plasmas. In each case the emitted or absorbed signal is produced by an approximately homogeneous plasma region.

laser-fusion implosion experiments, the observed x-ray signals consist of a superposition of contributions from a range of density-temperature conditions along the line of sight into the plasma. Such data can be compared with predictions of existing theory, but cannot easily be unfolded to yield accurate measurement of specific atomic processes. This difficulty is now solved, in principle, by the development of experimental geometries more favorable to scientific studies (Fig. 1).

In the plasma microdot technique (Fig. 1a) a small spot of high-Z (i.e., Z > 10) material is imbedded in a low-Z target such as plastic. Under irradiation the high-Z material expands as a plasma column, axially confined by the neighboring low-Z plasma, and strongly dominates the x-ray emission; a spectrometer observing this plasma from the side sees a unique density-temperature section of the high-Z plasma column. The technique has been applied to flow visualization (Herbst et al.[5]), plasma spectroscopy (Gauthier et al.[6]) and the verification of LASNEX hydrodynamic calculations (Rosen et al.[7]).

A similar technique (Fig. 1b) relies on a magnetic field to confine an expanding laser plasma at densities ~ $10^{18}/cm^3$. This steady plasma has been shown, using Thomson scattering, to be remarkably homogeneous and therefore an excellent source for plasma spectroscopy experiments (Crawford and Hoffman[8]).

A third geometry yielding a very dense plasma is the planar shock-wave technique (Fig. 1c). In this case, if one knows the material equation of state and measures the shock speed (e.g., in the stepped-target geometry shown), the laws of conservation of mass, momentum and energy enable one to uniquely determine the density-temperature conditions of the hot dense plasma. With proper selection of focal spot size and pulse length, one can realize a homogeneous steady plasma at densities greater than the initial solid density.[9] Interesting recent experiments with shock-produced plasmas include absorption spectroscopy (Bradley et al.[10]), measurement of electrical conductivity (Ng et al.[11]), and hydrodynamic studies with short-wavelength light (Fabbro et al.[12]).

These new experimental techniques, a worldwide proliferation of pulsed laser research facilities, and the strong scientific interest stimulated by the recent demonstration of a laser-pumped soft x-ray laser(7) together signal that dense plasma research will be very active in the next few years.

I. THERMAL IONIZATION

The most obvious result of laser heating is thermal ionization produced by electron impact and/or photoelectric absorption of x-rays.

The first general rule is a well-known characterization of plasma ionization in complete thermal equilibrium LTE:

G-1.) An equilibrium plasma ionizes to a charge state $Q(Z, \rho, T)$ at which

$$I(Z,Q) \simeq \xi\ kT \tag{1}$$

The coefficient ξ is a fundamental measure of plasma density effects.

In Eq. (1), Z = nuclear charge, Q = ion (average) charge state, $I(Z,Q)$ = ionization potential. ξ is essentially the electron entropy:

$$\xi = \ln\left(\frac{2}{n_e \lambda^3}\right) = S/k - \frac{5}{2} \tag{2}$$

where $\lambda = (2\pi\hbar^2/m_e kT)^{1/2}$ = electron thermal deBroglie wavelength; n_e = electron number density = $Q\rho/AM_p$; S = entropy per free electron; k = Boltzmann constant. Equations (1) and (2) follow from the Saha equation for plasma ionization (Zel'dovich and Raizer[13]); the derivation assumes equilibrium non-degenerate plasma conditions.

Figure 2 gives contour plots of the ionization state, the ratio I/kT and $\xi = \ln(2/n_e\lambda^3)$. One sees $\xi \simeq 10\text{-}15$ for low-density hot plasma, but $\xi < 5$ at dense-plasma conditions. It is evident that ξ and I/kT are approximately equal. The figures are based on the Thomas-Fermi cell model, but other theories give similar results.

The ionization potentials I(Z, Q) are the basic atomic data required to calculate equilibrium (LTE) ionization. There are two ways to obtain quick estimates of the ionization potentials: Thomas-Fermi theory,[3] or the Bohr model,

$$I_n = \frac{Q^2 e^2}{2a_o n^2} \tag{3}$$

which relates the ionization potential to the ion charge Q and the principal quantum number (= n) of the outermost bound electron.

Combining Eqs. (3) and (1) we find

$$Q \simeq \left(\frac{\xi\ n^2 kT}{13.6\ \text{eV}}\right)^{1/2} \propto T^{1/2} \tag{4}$$

as a scaling law for partial ionization in LTE. Equations (1)-(4) are used to compare physical processes; for example, the free electron specific heat $\simeq 3/2\ Qk$ is less than the ionization specific heat $\simeq I(Q)\ dQ/dT \simeq 1/2\ \xi Qk$ for a partially-ionized plasma with $\xi > 3$.

The scaling of Q with $T^{1/2}$ fails (i) for fully-ionized plasmas, where Q = Z; (ii) at low charge states, $Q < 1$; (iii) near closed-shell configurations, where Q is relatively independent of T over a range of temperatures; and (iv) at

FIG. 2. Thermal equilibrium (LTE) gold plasma calculated by the Thomas-Fermi cell model. Contours show ion charge Q, ionization potential I/kT and entropy parameter $\xi = \ell n (2/n_e\lambda^3)$. The close similarity of the latter two illustrates rule G-1.

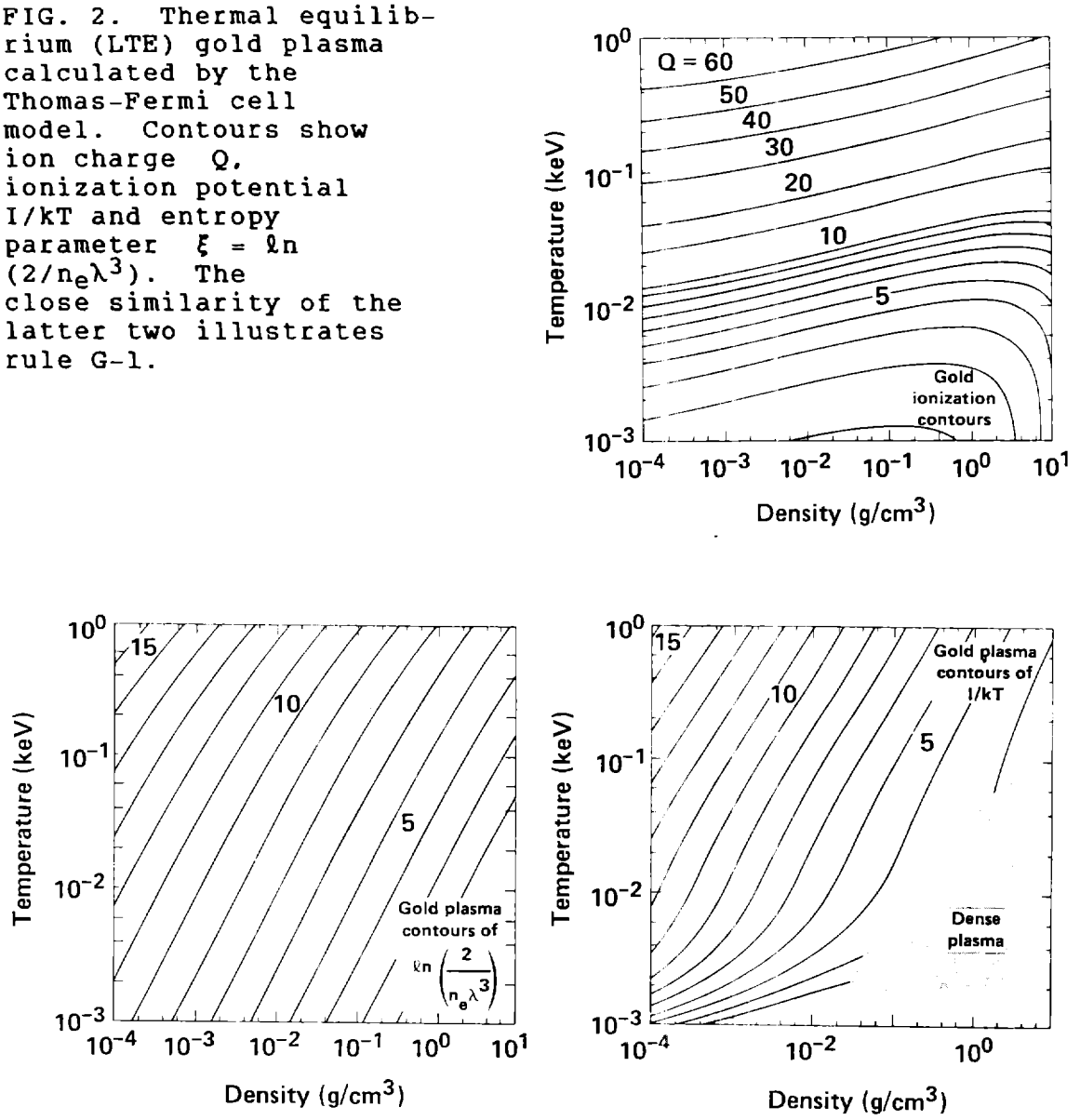

very high densities where degeneracy and pressure-ionization occur. The scaling also fails at low densities where most plasmas are optically thin and depart from thermal equilibrium. The scaling $Q \propto T^{1/2}$ is illustrated in Fig. 3.

Energy Level-shifts

Even for isolated ions, the energy-levels of core and valence electrons change as the ionization state increases. These changes are simply described by an algebraic screening model often used in fusion research. Let us examine a hypothetical Bohr orbit in a many-electron atom having average orbit radius r_n, velocity v_n. The assumptions of the Bohr theory are:

$$\frac{Q_n e^2}{r_n^2} = \frac{m v_n^2}{r_n} \quad , \quad m v_n r_n = n\hbar$$

The first relation expresses Newton's law (F = m a), the second the quantization of angular momentum. The solution

of these two equations is

$$r_n = a_o n^2/Q_n \tag{5}$$

$$v_n = Q_n e^2/n\hbar \tag{6}$$

The useful result of this simplified treatment is the idea that r_n and v_n depend upon an effective charge associated with the electric field at radius $r = r_n$, i.e., upon the inner screening charge

$$Q_n = Z - \sum_{m \le n} \sigma_{nm} P_m \tag{7}$$

Here P_m is the population of the m^{th} shell and σ_{nm} is a screening coefficient which tells what fraction of the charge of shell m resides inside radius r_n. In Eq. (7) the screened charge is assumed to be independent of subshell quantum numbers (j or ℓ) and a linear function of the populations.

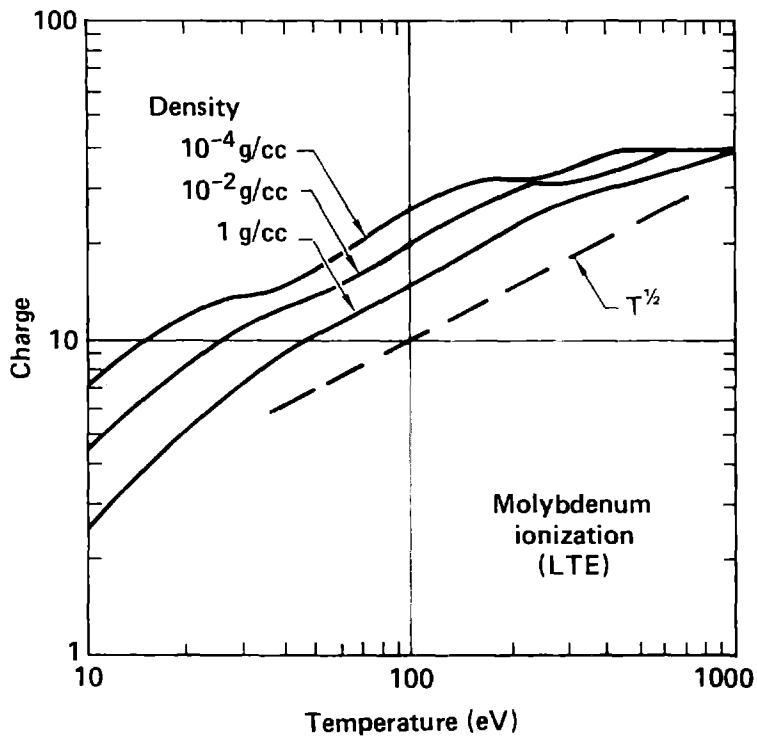

FIG. 3. Molybdenum charge state as calculated by the screened hydrogenic average-atom theory. The figure shows the scaling $Q \propto T^{1/2}$, and the tendency of Q to decrease with rising density in the nondegenerate density range. The ionization shelf structure at closed-shell configurations (Q = 40, 32, 14) disappears at high densities, illustrating rule G-7.

The energy E_n of the electron also involves the electrostatic potential V(r) at radius r_n.

$$E_n = \tfrac{1}{2}mv_n^2 - eV(r_n)$$

The potential V(r) has a contribution from outer screening: i.e., from electrons outside radius r_n. A useful approximation for this potential is:

$$V(r_n) = \frac{Q_n e}{r_n} - \sum_{m \geq n} \sigma_{mn} \frac{P_m e}{r_m}.$$

The first term is the potential outside a spherical core of charge + Q_n e, and the second term sums the potentials inside spherical shells of charge - σ_{mn} P_me located at radii $r_m > r_n$. With this model for the electrostatics,

$$E_n = -\frac{Q_n^2 e^2}{2a_o n^2} + \sum_{m \geq n} \sigma_{mn} \frac{P_m e^2}{r_m} \qquad (8)$$

The approximation based on Eqs. (7,8) is the screened hydrogenic model (Strömgren[14], Mayer[15], Lokke et al.[16], Zimmerman and More[17]). In this treatment, inner screening enters the calculation of Q_n, r_n and v_n, while outer screening affects only the potential $V(r_n)$ and energy E_n. Because of screening the one-electron eigenvalues E_n are strong functions of the ion charge-state (Fig. 4).

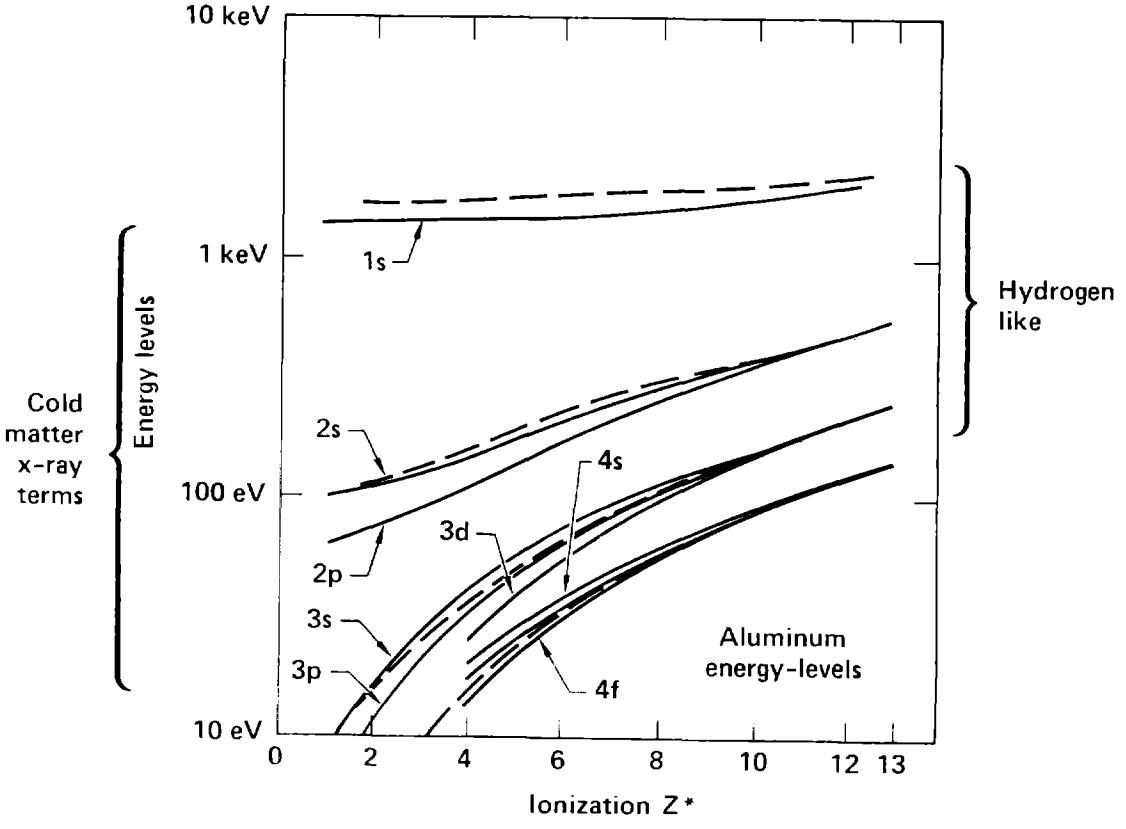

FIG. 4. Variation of Aluminum one-electron eigenvalues with ion charge. Dashed curves are the screened hydrogenic model, Eq. (8); solid curves are WKB eigenvalues for Thomas-Fermi ions. The calculations illustrate rule G-1a.

This simplified model is actually better than it appears at first sight for three reasons:

(1) One can optimize the choice of screening constants σ_{nm}, and thereby obtain a reasonable approximation to results of more accurate quantum calculations.[18]

(2) There is a Koopman's theorem which relates the one-electron energy-level E_n to a formal total ion energy of tractable functional form[17,18]

$$E_n = \frac{\partial E_{ion}}{\partial P_n} \tag{9}$$

with

$$E_{ion} = - \sum_n \left(\frac{Q_n^2 e^2}{2a_o n^2} \right) P_n = \sum_n E_n P_n - U_{ee} \tag{10}$$

Because of this result, one can employ E_{ion} as a model Hamiltonian which generates a consistent approximate statistical theory of the spectra of many-electron atoms.[3,17,18]

(3) Equations (5-8) are close cognates of more persuasive formulas obtained by simplification of the WKB theory of complex atoms. For example, the non- relativistic WKB theory yields an energy eigenvalue[18,19]

$$E_{n\ell} = - \frac{Q_n^2 e^2}{2a_o (n - \Delta_{n\ell})^2} + E_n^o$$

together with a precise specification of the inner-screened charge Q_n, the quantum defect $\Delta_{n\ell}$ and the outer-screening correction E_n^o. This WKB formula is close enough to the simpler model of Eq. (8) to give useful practical guidance in developing the model (Fig. 4).

Inner screening dominates the increase of the ionization potential I(Z,Q) with ion charge Q. On the other hand, outer screening is the reason why K-shell absorption or fluorescence energies change with removal of outer electrons.

Combining these ideas, we extend the rule G-1

G-1a.) Excitation energies are approximately proportional to $I(Z,Q) \propto kT$. Line spectra and absorption edges change with temperature to follow the maximum of the black-body spectrum.

The rule is illustrated by calculations of aluminum photoelectric absorption (Salzmann and Wendin[20]) based on Saha ionization-equilibrium calculations of the ion populations (Fig. 5).

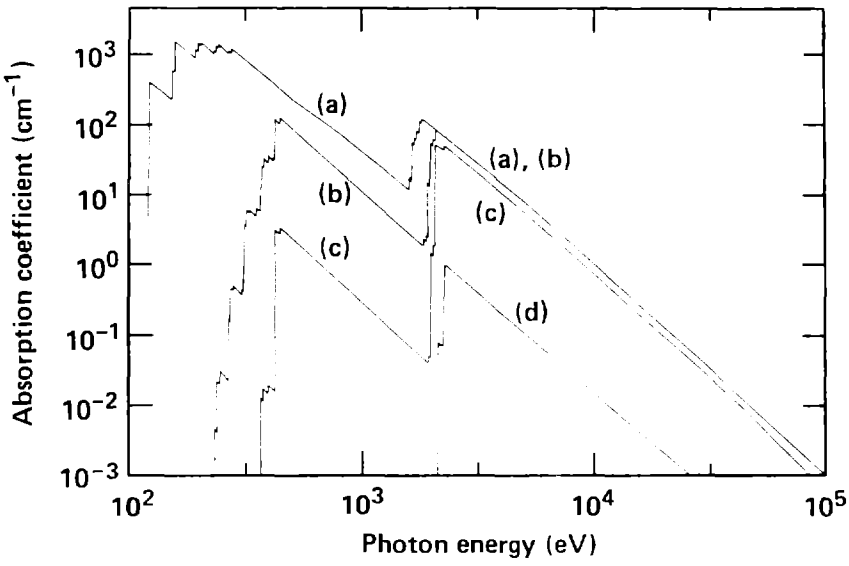

FIG. 5. Aluminum photoelectric absorption coefficient for density $n_i = 10^{21}/cm^3$ at temperatures a.) 32 eV, b.) 100 eV, c.) 320 eV, d.) 1000 eV (Salzmann and Wendin[20]). The motion of the effective absorption edge illustrates rule G-1a.

For fully-ionized plasmas, the thermal average (Rosseland) opacity has a temperature-dependence $\sim T^{-3}$ resulting from the $(h\nu)^{-3}$ dependence of the bremsstrahlung absorption cross-section.[21] For partially-ionized plasmas, the dominant photoelectric cross-section has the same frequency-dependence $(h\nu)^{-3}$, but the opacity now has a much weaker temperature- dependence $\sim T^{-1}$ due to the thermal shifts of photoelectric edges.

Shifts in energy-levels associated with ionization are much larger than any possible level-shift due directly to density itself. This point is important because the ionization state depends on density through Eq. (1). The density derivative $(\partial E_n/\partial\rho)_T$ includes a large red-shift associated with recombination while the derivative at constant charge state $(\partial E_n/\partial\rho)_Q$ is much smaller or zero.[22]

II. ION INTERACTIONS

The time-average distance between ions is obviously much greater than the ion size in low-density plasmas. Is this instantaneously true? Do ions touch during their thermal motion in the plasma?

The ion core radius R_i is related to the ionization potential I by

$$R_i(Z,Q) \propto Qe^2/I(Z,Q)$$

(this estimate is exact in Thomas-Fermi theory[3]) and for ions having thermal energies $\sim$ kT the minimum ion separation R_L is that for which

$$\frac{Q^2e^2}{R_L} \simeq kT$$

Together with Eq. (1) this implies

$$\frac{R_L}{R_i} \simeq Q\xi \gg 1 \tag{11}$$

especially for low-density plasmas where $\xi \gg 1$. Equation (11) says that ion cores are well-separated even during the closest encounters.* This in turn implies that the Coulomb law $U(R) = Q_1 Q_2 e^2/R$ is a good representation of the ion-ion potential.

For low-density (ideal) plasmas there are three length scales which describe ion spatial correlations:

$$\begin{aligned} R_L &= \text{Landau length} = Q^2e^2/kT \\ R_o &= \text{ion-sphere length} = (3/4\pi n_i)^{1/3} \\ D_i &= \text{(ion) Debye length} = (kT/4\pi Q^2e^2n_i)^{1/2} \end{aligned} \tag{12}$$

For the usual low-density plasma,[23]

$$R_L \ll R_o \ll D_i \tag{13}$$

When this inequality is satisfied, there are many ions in a sphere of radius D_i and the ion correlations are described by the Debye-Huckel theory. In this theory, a static point charge is screened within a length D given by

$$\frac{1}{D^2} = \frac{1}{D_i^2} + \frac{1}{D_e^2} = \frac{4\pi Q^2e^2n_i}{kT_i} + \frac{4\pi Qe^2n_i}{kT_e} \tag{14}$$

The first term corresponds to ion screening and the second to screening by free electrons. It is evident that ions dominate the static screening whenever $Q > 10$; this is the case for laser plasmas generated from SiO_2, Al, etc.

* The conclusion fails in dense plasmas where R_L is no longer the distance of closest approach, see Eq. (18) below.

In order to understand the ion correlations induced by Coulomb interactions, it is useful to examine the ion number density fluctuation $\langle \delta n_i^2(k) \rangle$ as a function of wave-vector k. In the Debye-Huckel theory (Salpeter[24]),

$$\langle \delta n_i^2(k) \rangle = \begin{cases} \frac{n_i}{V} \frac{D^2(k^2 + 1/D_e^2)}{1 + k^2 D^2} & \text{electron and ion screening} \\ \frac{n_i}{V} \frac{k^2 D_i^2}{1 + k^2 D_i^2} & \text{ions only } (T_e \to \infty) \\ \frac{n_i}{V} & \text{ideal gas without screening} \end{cases} \quad (15)$$

Figure 6 plots $\langle \delta n_i^2 (k) \rangle$ for a typical low-density plasma. One sees that Coulomb interactions tend to inhibit the long-wavelength charge-density fluctuations relative to those which would exist in an uncharged ideal gas. This suppression of fluctuations is the k-space image of the Debye screening itself.

We abstract a general principle from the example given in Fig. 6:

G-2.) Coulomb interactions tend to suppress (reduce) thermal fluctuations.

The argument for the general rule is the following: usually a non-interacting (ideal) many-body system has many highly degenerate states which are equally populated in thermal equilibrium. Coulomb interactions split this degeneracy; fewer low-energy states are populated more heavily and so the non-ideal gas has less thermal fluctuation.

The general rule is also illustrated by ion Stark broadening: Coulomb interactions between the plasma perturbers reduce the large microfields responsible for ion Stark wings in comparison with the non-interacting (Holtsmark) calculation (Ecker[25], Mihalas[26]). Another example: ion Doppler line-width is reduced when one includes the effect of Coulomb interactions between the ions (Dicke[27], Burgess and Lee[28]). Another example: calculations of ion charge-state distributions show that more rigorous models which include the electron-electron interactions predict less ionization fluctuation $\langle \delta Q^2 \rangle$ than a non-interacting average-atom model (Green[27], More[2]).

Ion Coupling

The numerical study of ion correlations in plasmas has centered around a standard idealized model, the <u>one-component</u>

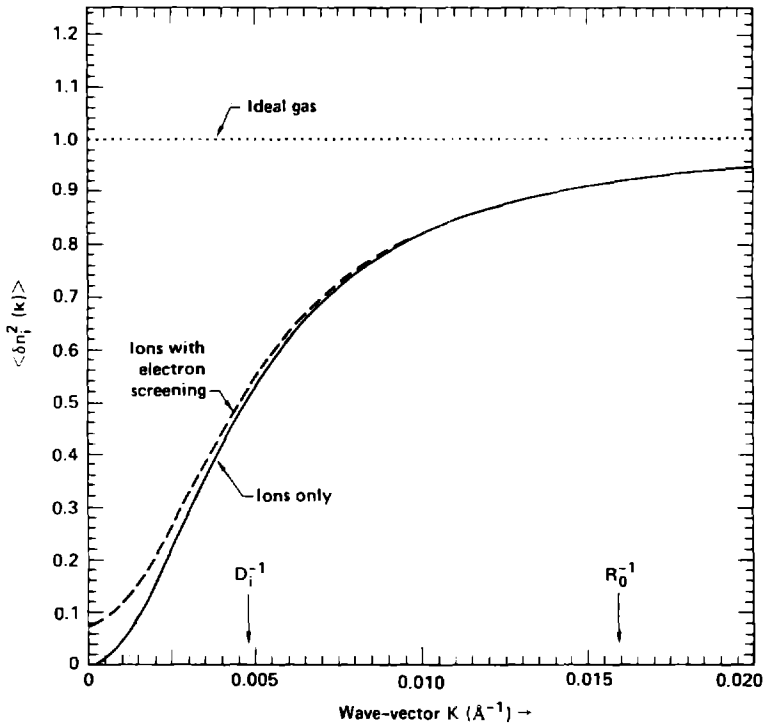

FIG. 6. Ion number-density fluctuation for a plasma with $n_i = 10^{18}/cm^3$, $Q = 10$, $T_e = 1$ keV and $T_i = .8$ keV. The large-scale charge fluctuations are strongly inhibited by Coulomb interactions, illustrating rule G-2. Electron screening reduces the effective Coulomb repulsion and permits some (neutral) density fluctuation.

plasma (Brush et al.[30], Hansen[31]). This is a model of classical point charges + Qe moving in a uniform fixed background of negative charge.

The equilibrium statistical mechanics of the one-component plasma is generated by the configurational partition function Z_c:

$$Z_c = \int d^3R_1 \int d^3R_2 \ldots \int d^3R_N \quad e^{-\sum_{i,j} \frac{Q^2e^2}{|R_i - R_j| kT}}$$

$$= R_o^{3N} \int d^3x_i \ldots \int d^3x_N \quad e^{-\Gamma \sum_{i,j} \frac{1}{|x_i - x_j|}}$$

In the second form, the integration variables are changed from ion positions $\vec{R}_i$ to scaled positions $\vec{x}_i = \vec{R}_i/R_o$, where $R_o = (3/4\pi n_i)^{1/3}$.

It follows that the configurational partition function depends essentially on only one variable, the ion coupling parameter Γ, defined by

$$\Gamma \equiv \frac{Q^2e^2}{R_o kT} \tag{16}$$

The ion coupling parameter describes the strength of ion correlations and controls the validity of different theoretical approaches. For weak coupling ($\Gamma \ll 1$) the Debye-Huckel theory is a good approximation. In this case the average Coulomb energy per ion is

$$\Delta E_c = -\frac{1}{2}\frac{Q^2e^2}{D_i} = -\frac{\sqrt{3}}{2}\Gamma^{3/2}\,kT \qquad (17a)$$

In the weak coupling case ($\Gamma \ll 1$) this energy is much less than the average thermal energy ~ kT, so the Coulomb forces are weak perturbations; the same conclusion is implied by the fact that many ions ($N \propto (D_i/R_o)^3 \gg 1$) are required to screen a test charge.

For strong coupling ($\Gamma \geq 0.5$) one has a nontrivial many-body problem which is well-suited to computer simulation. In this case the screening cloud around each ion involves a modest number of particles, so that a simulation using a few hundred computational ions becomes reasonably accurate.[31-33] The Monte Carlo (MC) simulations examine many configurations and weight the contributions by a Boltzmann factor corresponding to the total ion interaction energy (computational algorithms are described in Ref. 34). Molecular Dynamics (MD) simulations simply solve the classical equations of motion to generate time histories of the ion dynamics; physical quantities are calculated as time averages.

What are the effects of strong ion correlation? The rule G-2 goes directly to the heart of the question: ions repel each other and try to avoid close encounters. This forces them into an increasingly orderly arrangement which ultimately (for $\Gamma > 170$) becomes a crystalline state.

For $\Gamma > 1$, the ion-sphere model is not a bad approximation: each ion is surrounded by a cavity filled with electrons but devoid of neighbor ions. The cavity radius is ~ R_o; numerical simulations show that the nearest neighbor distance is $\simeq 1.7\,R_o$. The energy per particle is approximately

$$\Delta E_c \simeq -\frac{9}{10}\frac{Q^2e^2}{R_o} = -\frac{9}{10}\Gamma\,kT \qquad (17b)$$

which corresponds to the electrostatic interaction of a point ion with a uniform neutralizing electron gas in the ion-sphere volume. MC simulations have given more accurate values for this Coulomb energy $\Delta E_c(\Gamma)$.

An interesting feature of the strongly coupled plasma is the breakdown of Eq. (13). R_L, originally defined as the (energetic) distance of "closest approach," becomes greater than the average ion separation R_o. Indeed,

$$\frac{R_L}{R_o} = \Gamma > 1$$

In the strongly coupled plasma the ions are forced together against their Coulomb repulsions. The lengths R_L and D_i

become meaningless, and the single distance R_o serves as distance of closest approach, average pair-separation and screening length.

Simulations of the one-component plasma provide a variety of useful data. The Coulomb interaction energy ΔE_c enters the plasma hydrodynamic equation of state and the equilibrium ionization (ΔE_c generates the continuum lowering). The probability distribution for plasma electric fields $P(|\vec{E}|)$ can be obtained from the plasma simulations; this determines the ion Stark profile. The ion pair distribution g(r) gives the probability to find a neighbor ion a specified distance r away from one central ion; g(r) is used in calculation of quantum interference-scattering effects which arise in electrical conductivity or plasma bremsstrahlung emission.

Charge-state Variations

The one-component plasma is an idealized model; although it is very useful it also omits certain physical processes. Among these are phenomena associated with changes in the ion charge Q.

For real plasmas the time-averaged ion charge $Q = Q(\rho,T)$ is dependent upon density and temperature and this means that care must be exercised in adapting results from the OCP simulations (e.g., integrating the OCP specific heat with respect to temperature).

For temperatures much below the Fermi temperature, the ion charge depends only upon density, $Q(\rho,T) \simeq Q(\rho,0)$. Examination of Thomas-Fermi calculations for degenerate matter shows that a rather accurate description of this pressure ionization is given by[3]

$$R_i(Z,Q) \simeq R_o \tag{18}$$

which determines the plasma ionization state $Q(\rho)$ at low temperatures in terms of the ion core radius $R_i(Z,Q)$ and ion-sphere radius R_o. With this equation one sees that ion cores indeed come into close contact in degenerate high-density matter.

In the nondegenerate range the plasma ionization state is proportional to $T^{1/2}$ according to Eq. (4). Laughlin has pointed out that this power law implies that Γ is essentially independent of temperature in a partially-ionized plasma.[35] This means that ion thermal motion (e.g., amplitude of ion vibration with respect to the neighbors) is approximately independent of temperature; the potential between ions grows stronger as rapidly as the thermal energy does.

The ion charge also changes with time through ionization and recombination and this causes interesting new effects in the ion dynamics.

We will describe one such process, a Raman effect in electron-ion energy exchange, which is predicted theoreti-

cally for partially-ionized plasmas and caused by sudden charge fluctuations occuring in ionization and recombination.[2,36,37] The effect is a dense-plasma process, but is quantitatively important at surprisingly low plasma densities where it affects the viability of one well-known x-ray laser scheme.

In this case, the pumping efficiency of a resonant photopumped laser depends strongly on the Doppler linewidth, which is determined by the ion temperature T_i, controlled in turn by the heat exchange between electrons and ions (Hagelstein[37]).

Collisional Heating of Ions

Ordinarily the electron-ion heat exchange is calculated from the Landau-Spitzer formula,[23,38]

$$\frac{dE_i}{dt} = \frac{m_e}{M_i} (kT_e - kT_i)\, n_e \sigma_{eff} v_e \qquad (19)$$

where E_i = energy per ion; m_e, M_i = electron, ion mass; kT_e, kT_i = electron, ion temperatures; n_e = electron number density; $v_e = (kT_e/m_e)^{1/2}$ = electron thermal velocity; and

$$\sigma_{eff} = 4\sqrt{2\pi}\, \left(\frac{Qe^2}{kT_e}\right)^2 \log \Lambda \qquad (20)$$

is an effective collision cross-section. The numerical coefficient in Eq. (20) comes from a well-known formula for the electron-ion coupling time τ_{ei} (Spitzer[23]). Equations (19)-(20) describe energy transfer occuring in electron-ion collisions; a small fraction (proportional to $m_e/M_i \ll 1$) of the kinetic energy of the hotter particle is transferred in each Coulomb collision.

Ionization Heating of Ions

The Raman heat-exchange mechanism is also a consequence of electrical forces. Consider an ion of charge +Qe, surrounded by a neutralizing or screening cloud of electrons and ions. The electrical energy stored in this screening cloud is $\Delta E_c \sim Q^2e^2/R_s$, where R_s is the appropriate screening length.

After electron impact ionization, the screening cloud must adjust to the increased ion charge $Q' = Q + 1$. For a time short compared to the ion plasma oscillation period $(1/\omega_{pi})$ the extra unit charge is screened by electrons at a large distance $\simeq D_e$ = electron Debye length. At the radius R_o of the nearest neighbor ions this leaves an unscreened electric field which causes the neighbors to relax outward from the central ion. This outward motion is rapidly thermalized into ion kinetic energy. Thus in each ionization event the ions gain a thermal energy of order $d(\Delta E_c)/dQ \sim Qe^2/R_s$.

This reasoning gives an estimate[2]

$$\frac{dE_i}{dt} \simeq \frac{Qe^2}{R_s} \varphi\, n_e \sigma_{ii} v_e \qquad (21)$$

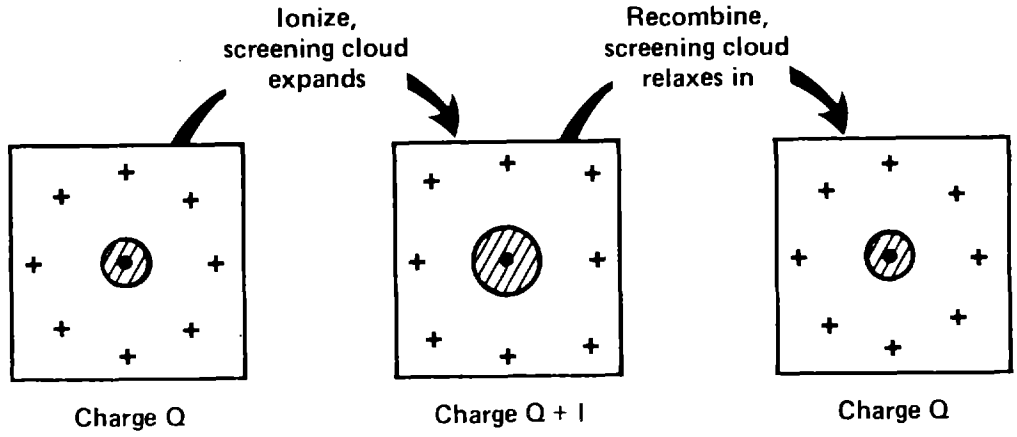

FIG. 7. Schematic representation of electron-ion energy exchange during ionization.

for the rate of ion heating associated with the ionization process. The rate of energy exchange is proportional to the rate of impact ionization $n_e \sigma_{ii} v_e$, and φ is a numerical factor intended to correct for the possibility of recombination occuring before completion of the changes in the ion screening cloud.

It is important to observe that the energy transfer is not necessarily cancelled by a subsequent recombination event. Indeed, if the time between ionization and recombination exceeds $1/\omega_{pi}$, and if T_i is sufficiently low, the screening cloud around the ion of charge Q + 1 has time to relax into a low-energy configuration; when recombination occurs, the screening cloud must again re-adjust and this transfers additional energy to the ion system.

A very similar heat-exchange mechanism is proposed by Hagelstein, who terms it ion proximity heating.[37]

Using Eqs. (19),(21) we can compare the Raman or proximity heating to the collisional energy-transfer: the ionization cross-section is usually much smaller than the Coulomb cross-section but the energy exchanged per ionization event ($\sim Qe^2/R_s$) can greatly exceed the small energy transfer ($\sim m_e k T_e/M_i$) in a collision.

The process described by Eq. (21) is analogous to phonon emission occuring in the absorption of visible light by impurities or color centers in transparent solids.[39] In that case absorption raises the defect center to an excited state which interacts with the crystal with an altered potential; in relaxing to the groundstate configuration in this potential the defect center releases energy as phonons. This produces a classic optical Raman effect: emission is red-shifted relative to absorption. Equation (21) describes an electronic analogue of this process.

After estimating the ion temperature rise caused by this mechanism in a rapidly ionizing plasma, we reconsider Eq. (21) to reconcile it with the principle of detailed balance.

Example: A Rapidly Ionizing Plasma

The importance of the ionization heat-exchange is illustrated by one recently proposed design for a laser-pumped soft x-ray laser.[37] In this experiment a low ion temperature ($T < 10$ eV) would have the favorable consequence of reducing the Doppler width of the pumping transition. In one specific proposal neon ions at a number density $\sim 10^{18}/cm^3$ would be rapidly stripped to charge $Q = +8$ by photoelectric absorption of kilovolt x-rays from an intense laser-plasma source. For the proposed plasma conditions one has $kT_i \simeq 1 - 5$ eV and $kT_e \simeq 60 - 200$ eV. With these assumptions, the screening lengths defined by Eqs. (12, 14) are:

$$R_o \simeq 60 \text{ Å}$$

$$D_i \simeq 10\text{-}20 \text{ Å}$$

$$D_e \simeq 200\text{-}400 \text{ Å}$$

Since $D_i \ll R_o$ one has a strongly coupled plasma despite the relatively low ion density.

In the ion-sphere description of this strongly coupled plasma, the central ion is assumed to be surrounded by an electron gas which is nearly uniform in the range $0 < r < R_o$; outside this range the other ions and electrons are taken to comprise a uniform neutral plasma.

When an ion of arbitrary charge Q' is placed in this plasma, it will repel neighbor ions in order to produce a cavity containing only electrons, whose radius is such as to assure electrical neutrality. The screening energy is then $\Delta E_c = 9/10\ (Q'^2e^2/R')$ with $Q' = (4\pi/3)\ R'^3\ n_e$ and constant free electron density n_e determined by the average ionization state $\langle Q' \rangle$. When we include the change of cavity radius with ionization of the central ion we find

$$\left(\frac{\partial \Delta E_c}{\partial Q'}\right) = \frac{3}{2}\frac{Q'e^2}{R_o}$$

A minimal ion temperature can be calculated by integrating these energy changes with respect to Q' from $Q' = 0$ to the final charge state $Q' = Q$. Assuming an ideal-gas ion specific heat we find:

$$kT_i \geq \frac{1}{2}\frac{Q^2e^2}{R_o}\, e^{-R_o/D_e} \qquad (22)$$

This mechanism alone thus predicts $kT_i \geq 7$ eV for the case considered. The actual ion temperature would be higher still because of the collisional heat transfer of Eqs. (19,20) and because of cyclic Raman heating occuring when the steady-state ionization is achieved.

The limitation indicated in Eq. (22) applies to a plasma composed of a single substance (e.g., pure neon). If this

material were diluted with a low-Z impurity (e.g., hydrogen gas) the same ion heating energy could be shared with more nuclei resulting in a lower ion temperature.

A Question of Detailed Balance

The formulation of electron-ion heat exchange based on Eq. (21) suffers from one significant defect: it appears to predict a continuous heating of the ions and thus appears to predict that the ion temperature T_i continues to rise even when $T_i > T_e$. This cannot be correct: the heat exchange mechanism must move the two species toward thermal equilibrium and the net rate of heat transfer must approach zero as the temperature difference approaches zero (see rule G-10).

This formal requirement (associated with detailed balance) is certainly satisfied by the collisional heat-transfer described by Eq. (19).

In order to resolve this question for the Raman process it is useful to consider ionization and recombination occuring in the presence of a fluctuating electrostatic potential Φ produced by plasma particles near a central ion.

Ionization, Recombination in a Potential Φ

We consider an ion subject to a potential Φ generated by the neighboring charged particles. If the plasma density is sufficiently low the nearest neighbor ion is often the main source of this potential, whose magnitude is therefore $\sim Qe/R_o$; for definiteness the reader may consider this case while noting that the reasoning is independent of the source of the potential.

It is assumed that the spatial variation of the potential Φ is on a size-scale much larger than the ion radius R_i and the time variation is slow compared to electron transit times. An electron of energy gains a kinetic energy = $e\Phi$ as it approaches the central ion, and the modified impact ionization cross-section is therefore approximately $\sigma_{ii}(\epsilon_o + e\Phi)$, where $\sigma_{ii}(\epsilon_o)$ was the original cross-section for impact ionization without the potential.

After ionization there are two low-energy free electrons. One or both could be at low kinetic energies ($\epsilon < e\Phi$) where they are actually loosely bound by the plasma fluctuation. However electrons in this portion of phase-space are extremely collisional and therefore may still be regarded as free.

The ionization rate is affected by a change in the distribution function for the incident free electron and by the probability of finding the target ion in its specified charge state. Assuming the ion probabilities are determined by an equilibrium Boltzmann factor proportional to $\exp(-Qe\Phi/kT_i)$, and assuming the electron distribution is a nondegenerate Maxwellian function of the asymptotic energy ϵ_o, the result is a modified ionization rate containing

the Boltzmann factors $\exp(e\Phi/kT_e - Qe\Phi/kT_i)$ and a cross-section evaluated at the shifted energy $\tilde{\epsilon}_o = \epsilon_o + e\Phi$.

The three-body recombination which is the time-reverse of this ionization also has an altered rate and the changes are slightly different. In this case the distribution functions contribute Boltzmann factors

$$\exp(2e\Phi/kT_e - (Q + 1)e\Phi/kT_i)$$

corresponding to two electrons incident upon an ion of charge Q+1. The 3-body cross-section is also evaluated at modified energies determined by energy conservation. Again there is a question about the low-energy portion of electron phase-space where one or both incident electron(s) could be formally bound to the potential fluctuation; again it seems reasonable to assume these electrons are in equilibrium with the adjacent positive-energy states.

If ion densities are determined by the LTE Saha equation containing the electron temperature, the ratio of recombination and ionization rates becomes

$$\exp[e\Phi(\frac{1}{kT_e} - \frac{1}{kT_i})] \tag{23}$$

Because this ratio is not unity for $T_i \neq T_e$, the Saha population ratios are altered when the temperatures are unequal. An effect of this character has previously been predicted.[40]

Using the corrections described we can readily form the rate of electron-ion energy exchange,

$$\frac{dE_i}{dt} = \langle e\Phi\{1 - \exp[e\Phi(\frac{1}{kT_e} - \frac{1}{kT_i})]\ n_e\sigma_{ii}v\rangle \tag{24}$$

The average is taken over configurations of the local environment and over the distribution function of the incident electron. The recombination contribution was related to the ionization rate as described above, using the LTE Saha detailed-balance condition. If we expand Eq. (24) assuming the potential $e\Phi$ to be smaller than either kT_e or kT_i, we find

$$\frac{dE_i}{dt} \simeq \langle (e\Phi)^2\rangle\ (\frac{1}{kT_i} - \frac{1}{kT_e})\ \langle n_e\sigma_{ii}v\rangle \tag{25}$$

This expression is a generalization of Eq. (21) for the case of nearly equal electron and ion temperatures; it predicts zero heat transfer at equilibrium and changes sign with the temperature difference. In the other limit ($kT_i \ll kT_e$) Eq. (24) is qualitatively equivalent to Eq. (21) and so this more comprehensive approach resolves the difficulty associated with the requirement of detailed balance.

The discussion given here refers to the process of impact ionization and 3-body recombination. A similar coupling of electron, ions and photons arises from photoionization and radiative recombination.

III. CORE INTERACTIONS AND PRESSURE IONIZATION

The ultimate dense plasma occurs inside white dwarf stars, at densities $\sim 10^6$ g/cm^3 ; all bound electrons are liberated, leaving point nuclei imbedded in a homogeneous degenerate electron gas. The electron gas is increasingly ideal as its density rises, because the kinetic energy per electron increases as $E_f \sim \rho^{2/3}$, more rapidly than the electrostatic energy $\langle Ze^2/r \rangle \sim \rho^{1/3}$.

Although the Chandrasekhar (degenerate) gas model applies to densities far beyond the laboratory range,[21] one finds similar behavior for the outer (valence) electrons in matter at less extreme densities:

G-3.) Strong compression raises electron kinetic energies relative to potential energies (i.e., high pressure "liberates" electrons as it crushes them down into smaller volumes).

The rule is illustrated by the virial theorem:

$$3pV = 2K + U \qquad (26)$$

For a cold, low-density system the pressure p is small and one has the isolated-atom result, $K \simeq -1/2\ U$. At high densities the Coulomb energy U becomes small compared to the kinetic energy K and one obtains the ideal gas law $K \simeq 3/2\ pV$ (this form is valid in degenerate or nondegenerate cases).

The virial theorem is often used in calculation of high-density plasmas so it is worth comment that Eq. (26) is valid only in certain circumstances. Equation (26) is correct for an isolated quantum system. It is also valid when applied to one unit cell of a periodic system such as a crystalline solid. In these cases there is no difficulty deciding how much kinetic or potential energy belongs to the volume V and the wave-functions obey boundary conditions which assist the required integration by parts.

In a dense plasma each atom (ion) is surrounded by a random environment of neighbor atoms without high symmetry or sharp boundaries. This situation is often described by the cell model: one nucleus located at the center of a spherical cavity in a uniform positive charge background (Liberman[41]). The cavity radius ($= R_o$) is set by the density (Fig. 8). The electron distribution is calculated by finite-temperature self-consistent field theory. A similar physical picture is assumed by the Thomas-Fermi or Thomas-Fermi-Dirac (TFD) cell models. Several authors have explored more elaborate prescriptions for the exterior positive charge density (Perrot[42], Cauble et al.[43]).

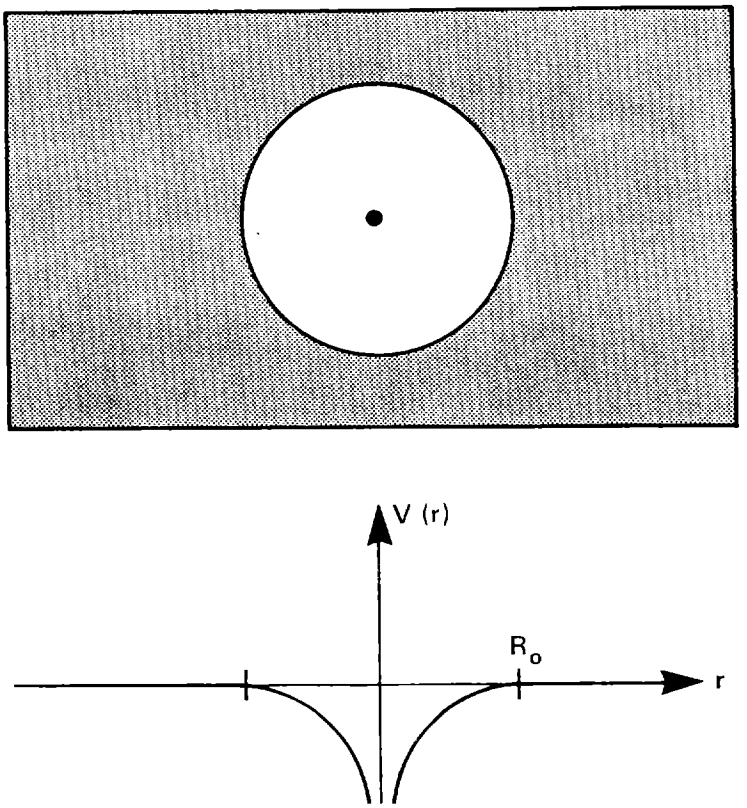

FIG. 8. Schematic representation of the spherical-cell model. A nucleus of charge Ze is located at the center of a cavity of radius R_o in a positive charge background $\rho+(r)$. The cavity radius is fixed by the matter density. The electron distribution is calculated from a self-consistent average potential V(r) and the chemical potential is chosen so that the cell is electrically neutral.

For the spherical-cell self-consistent field theory, we can establish an extended virial theorem referring to the atomic or cavity volume V_{at}:

$$3pV_{at} = K_{(1)} + K_{(2)} + U \tag{27}$$

with

$$K_{(1)} = \frac{\hbar^2}{2m} \sum_s f_s \int_{V_{at}} |\nabla\psi_s|^2 \, d^3r$$

$$K_{(2)} = -\frac{\hbar^2}{2m} \sum_s f_s \int_{V_{at}} \psi_s \nabla^* \psi_s^2 \, d^3r$$

In Eq. (27), ψ_s = wave-function in the self-consistent potential (the sums run over all one-electron states, bound and free) and f_s = Fermi function describing the occupation

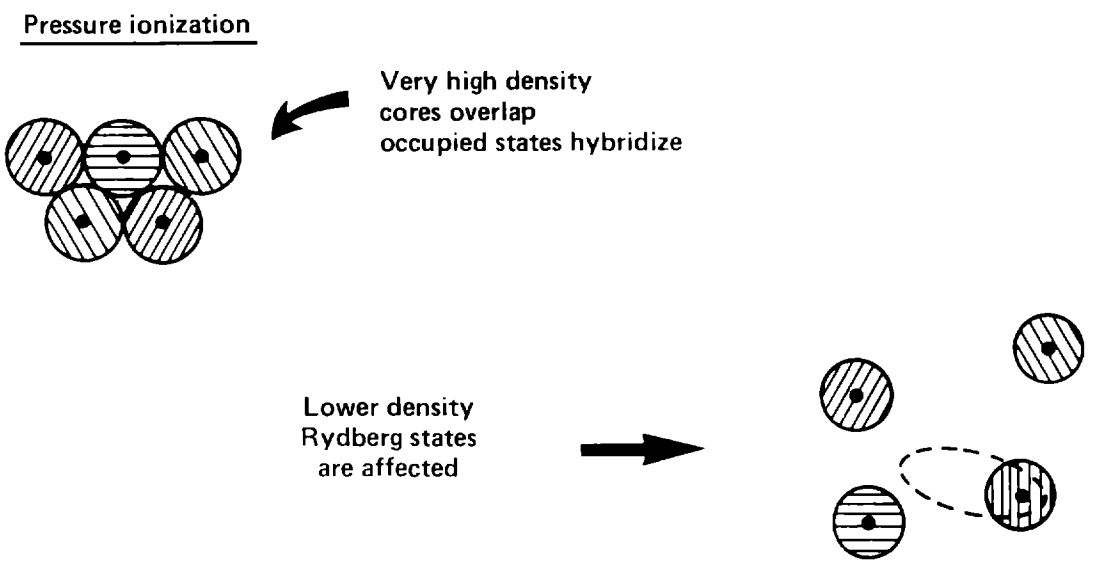

FIG. 9. Pressure ionization affects occupied or unoccupied eigenstates, depending upon the density.

of ψ_s. The pressure p appearing on the left side of the equation is equal to $P_{rr}(R_o)$, the radial element of the quantum kinetic stress or pressure tensor evaluated at the ion-sphere boundary.[44]

Pressure Ionization

The great difference between atomic structure for isolated atoms (ions) and those in the dense plasma is the importance of the continuum in the latter case. With increasing density, an increasing number of bound states are shifted into the continuum.

At high densities, pressure ionization occurs when ion cores are forced together; the outermost bound states hybridize and become propagating waves. At these densities atoms are arranged in a relatively regular close-packed structure and so ideas of solid-state band structure are directly applicable. The effective ion charge $Q(\rho)$ is approximately determined by Eq. (18) in this case.

At lower densities pressure destroys excited states which are only occasionally occupied. In this case the atoms are separated from their neighbors by random distances, and the fluctuations in the local environment probably play an important role. The low-density precursor of pressure ionization may be seen in the interactions between Rydberg atoms.

One requires a simple estimate of the density at which a given level is pressure-ionized, but this immediately raises questions and there is disagreement in the literature. We will summarize the most popular viewpoints and evaluate the formulas for a representative plasma (Table I). The reader will find further discussion in unpublished reports of Burgess,[45] Peacock,[46] and Brush and Armstrong.[47]

1.) Ion-sphere model (Unsold,[48] Carson et al.,[49] More and Zimmerman,[17] More,[18] Burgess and Lee[50]):

$$r_n \simeq 1/3\ R_o \tag{28}$$

Here r_n = orbit radius, Eq. (5); R_o = ion-sphere radius, Eq. (12). This formula follows from several lines of reasoning: it is the criterion for significant overlap of wave-functions on adjacent ions, it follows from a comparison of the binding energy and the continuum lowering, and it corresponds to a density at which the nuclear attraction for the electron is exceeded by the electric field of a neighbor ion.

2.) Debye-Huckel model (Rogers et al.,[51] Weisheit and Shore,[52] Vinogradov et al.[53]):

$$r_n \simeq D \tag{29}$$

For the case examined in Table I this criterion predicts many more bound states than does Eq. (28). Equation (29) is derived by locating the highest boundstate of the Debye-screened potential $V_{DH}(r) = (Qe/r)\exp(-r/D)$. The question is the validity of $V_{DH}(r)$ when used for this purpose.

3.) In the white-dwarf literature, one occasionally sees a mysterious criterion[54]

$$\epsilon_n \simeq E_f \tag{30}$$

This criterion must be intended to refer to degenerate plasmas. If applied to the nondegenerate plasma of Table I, Eq. (30) predicts an enormous number of bound states.

4.) Planck-Larkin method (Rogers[55]). This formula reduces or removes the contribution of bound-states obeying $|E_n| < kT$; for the plasma of Table I this translates to $n_{max} = 2$, a strange or bizarre result. However the Planck-Larkin formula is properly used only in thermodynamic calculations, and the continuum states are also modified so as to essentially replace the removed bound-electron contributions. For dense plasmas the calculations by the Planck-Larkin method often agree with Thomas-Fermi results to surprisingly high precision (see Table II).

5.) Landau-length model. In ideal plasmas satisfying Eq. (13), it appears that bound states having orbit radii comparable to $R_L = Q^2e^2/kT$ would eventually be strongly perturbed by close approach of a neighbor ion. This does not mean that states having $r_n > R_L$ would not generate (broadened) emission lines.

6.) Inglis-Teller limit. For sufficiently large quantum numbers the Stark effect will cause adjacent levels

to overlap in energy and make unresolvable contributions to the emission or absorption spectrum (Griem[56]). This occurs at

$$E_{n+1} - E_n \simeq r_n \left(\frac{Qe^2}{R_o^2}\right) \quad \text{or} \quad r_n \simeq \frac{R_o}{\sqrt{n}} \tag{31}$$

As the table shows, the predictions of these six models span a large range.

TABLE I.

Pressure ionization by various criteria for an Aluminum plasma at T = 1 keV, electron density $n_e = 10^{19}/cm^3$

MODEL	n_{max}
Ion sphere model	24
Debye-Huckel model	70
Fermi energy model	870
Planck-Larkin formula	2
Landau length	8
Inglis-Teller	19

At present there is no experimental evidence which would clearly select between the models. It appears that the most convincing theoretical arguments favor the ion-sphere picture.[18] Without repeating this discussion in detail, we summarize the main points:

a.) For strongly-coupled plasmas ($\Gamma > 1$) the ion-sphere picture is essentially required by our knowledge of ion correlation; in this case the Debye length has no physical interpretation. In spherical cell SCF calculations, bound-states reach zero binding energy and become resonances at a density determined approximately by Eq. (28) with the coefficient 1/3 as given.[44]

b.) For lower densities ($\Gamma < 1$) the question concerns the existence of discrete bound states having $R_o < r_n < D$, i.e., large orbits which encircle many ions. According to the Debye model, electrons in such states experience a weak spherically symmetric potential $V_{DH}(r) = (Qe/r)\ \exp(-r/D)$ which is known to be the average of the actual potential of the plasma. However the fluctuations from this average are very strong; the neighbor ions give rise to potentials $\sim .8\ Qe/R_o$ which greatly exceed $V_{DH}(r)$ for $r \gg R_o$. In particular, the electron mean free path for scattering by these potential fluctuations is less than the orbit circumference for hypothetical bound-states with

$R_o < r_n < D$; it is difficult to believe that a discrete quantized spectrum exists under these conditions.

Continuum lowering

The mechanism of pressure ionization is at least partially understood as continuum lowering: as the density rises the spatial average $\langle V(r) \rangle$ of the electrostatic potential becomes increasingly negative until it ultimately exceeds the free-atom binding energy of any given electron.

In the calculation of ionization balance, one generates this effect automatically if the Coulomb interaction energy per ion,

$$\Delta E_c = -a \frac{Q^2 e^2}{R_s}$$

(a = numerical coefficient, R_s = screening length) is added to the energy or free energy of the system. For low densities ($\Gamma \ll 1$) one assumes $a = 1/2$, $R_s = D_i$; for strongly coupled plasmas one has the ion-sphere form with $a = 9/10$, $R_s = R_o$.

The ionization process may be thought of as a change of Q occuring at constant free electron density n_e. Following the reasoning already presented near Eq. (22) the continuum lowering is then (for $\Gamma > 1$)

$$\left(\frac{\partial \Delta E_c}{\partial Q}\right)_{n_e=\text{const}} = \frac{3}{2} \frac{Qe^2}{R_o} \qquad (32)$$

This value is also the spatial average of the ion potential $V_i(r) = Qe/r$ over the ion-sphere volume, but not the average of the complete potential

$$V(r) = \frac{Qe}{r} + \frac{1}{2} \frac{Qe}{R_o} \left(\frac{r}{R_o}\right)^2 - \frac{3}{2} \frac{Qe}{R_o}$$

which includes the contribution of a uniform free-electron gas.

Interpolation between ion-sphere and Debye-Huckel screening formulas is most often accomplished with the Stewart-Pyatt model.[57] However this approach has certain defects and a completely satisfactory theory does not yet exist.[2]

Resonances and Pressure Ionization

In quantum spherical-cell SCF calculations, the effect of high pressure is to lower the continuum successively through various one-electron boundstates.

Above a density $\rho_{n\ell}$ the boundstate of energy $E_{n\ell}$ becomes a scattering resonance or shape resonance in the partial-wave potential

$$V_\ell(r) = V(r) + \frac{\hbar^2}{2m} \frac{\ell(\ell+1)}{r^2}$$

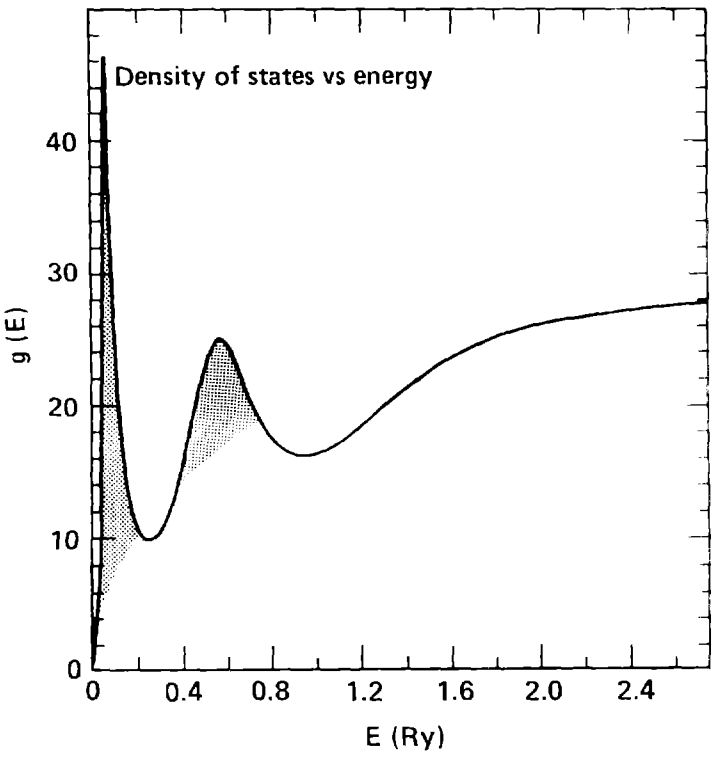

FIG. 10. Theoretical electronic density of states for aluminum calculated by the self-consistent field model (D. Liberman provided these data). Shading has been applied to enhance the contrast of 3p and 3d resonances from the $\epsilon^{1/2}$ background continuum density of states. The density is 2.7 g/cm^3 and the temperature is 50 eV.

which has an interior well and a barrier at $r \approx R_0$ associated with the centrifugal potential. According to scattering theory, the pressure-ionized state is described as a resonance state of complex energy

$$\tilde{E}_{n\ell} = E^0_{n\ell} + i\,\Gamma_{n\ell} \tag{33}$$

The real part $E^0_{n\ell}$ indicates the central energy of the resonance; the imaginary part $\Gamma_{n\ell} = \hbar / \tau_{n\ell}$ determines the resonance width or lifetime $\tau_{n\ell}$. The precise definition of the complex energy $\tilde{E}_{n\ell} = \hbar^2 Q^2_{n\ell}/2m$ is that there exists a solution $\phi_{n\ell}(r)$ of the radial Schroedinger equation which obeys the boundary conditions

$$\phi_{n\ell}(r) \rightarrow 0 \qquad r \rightarrow 0$$

$$\phi_{n\ell}(r) \rightarrow i^{\ell} N_{n\ell} e^{-iQ_{n\ell}r} \qquad r \rightarrow \infty \tag{34}$$

The normalization $N_{n\ell}$ of these wave-functions is fixed by a remarkable formula which is the analytic continuation of the boundstate normalization formula and which implies the first-order resonance perturbation theory,[58]

$$\delta\tilde{E}_{n\ell} = \int_0^{R_o} \phi^2_{n\ell}(r)\ \delta V(r)\ dr \qquad (35)$$

where $\delta V(r)$ is an arbitrary change in the potential. Equation (35) gives a unified expression for the perturbation in $E^{Q}_{n\ell}$ and $\Gamma_{n\ell}$.

In terms of these resonance energies one can transform the well-known expression for the continuum density of states

$$g(\epsilon) = c_i V\sqrt{\epsilon} + \frac{2}{\pi}\sum_{\ell}(2\ell+1)\frac{d\delta_\ell}{d\epsilon} \qquad (36)$$

to a simple and general form[44]

$$g(\epsilon) = c_1 V\sqrt{\epsilon} + \frac{b}{\sqrt{\epsilon}} + \sum_{n\ell} 2(2\ell+1)\ \mathrm{Re}\left[\frac{1}{i\pi}\frac{1}{(\epsilon-\tilde{E}_{n\ell})}\sqrt{\frac{\epsilon}{\tilde{E}_{n\ell}}}\right] \qquad (37)$$

The derivation of Eq. (37) uses a representation of the scattering matrix (S-matrix) originally proven by Regge;[59] it is rigorously correct for one-electron nonrelativistic potential-scattering theory.

When a state is pressure ionized, its binding energy approaches zero and moves to positive energies where it begins as a very narrow resonance. For such a state, the right-hand side of Eq. (37) gives a sharp resonance peak very similar to the delta-function contributions of the bound states.

Resonances at higher energies become broad and the contributions overlap and merge. Using the Born approximation for the scattering phase-shift, one can show that at high energies Eq. (36) gives

$$g(\epsilon) = c_1 V\sqrt{\epsilon} + \frac{c_1 V}{2\sqrt{\epsilon}}\Delta E + \ldots \qquad (38)$$

This corresponds simply to a continuum lowered by

$$\Delta E = \frac{1}{V}\int_0^{\infty} 4\pi r^2 V(r)dr \qquad (39)$$

From Eq. (37) one can calculate the average thermal population of a resonance state. The result is[44]

$$P_{n\ell} = 2(2\ell+1)\ \mathrm{Re}\left[\frac{1}{i\pi}\int_0^{\infty}\sqrt{\frac{\epsilon}{\tilde{E}_{n\ell}}}\ \frac{f(\epsilon)d\epsilon}{\epsilon-\tilde{E}_{n\ell}}\right] \qquad (40)$$

This is not exactly a fermi function because the resonance state is not exactly an eigenstate. Nevertheless Eq. (37) shows the various resonances make independent additive contributions to the total number of electrons in the continuum.

These resonance formulas give the most precise description of pressure ionization in the spherically symmetric cell model. A much more complex picture would emerge if we could perform calculations for models

containing a cluster of atoms. Perhaps some progress along these lines can be made through perturbation theory, based for example upon Eq. (35).

IV. QUALITATIVE BEHAVIOR OF DENSE PLASMAS

Electron-ion coupling

The interaction of ions with free electrons is measured by a coupling parameter defined as

$$\Gamma_{ei} = \frac{Qe^2}{R_o kT} \tag{41}$$

This is the ratio of potential energy $\sim Qe^2 / R_o$ to kinetic energy $\sim kT$ evaluated for an electron at the ion-sphere (interatomic) boundary. Of course, electrons closer to the ion interact more strongly, but the spatial average $\langle Qe^2 / rkT \rangle$ is proportional to Γ_{ei}.

Assuming the definition Eq. (41) one can show:

$$\Gamma_{ei} \leq 0.54 \text{ all } \rho, T \tag{42}$$

for hydrogen plasma described by the Saha equation. This surprising result is established in Appendix A. It is a rigorous consequence of the Saha equation, but that theory breaks down at high plasma densities (see G-5a).

The inequality (42) can be generalized,

G-4.) The interaction of ions with free electrons never becomes large.

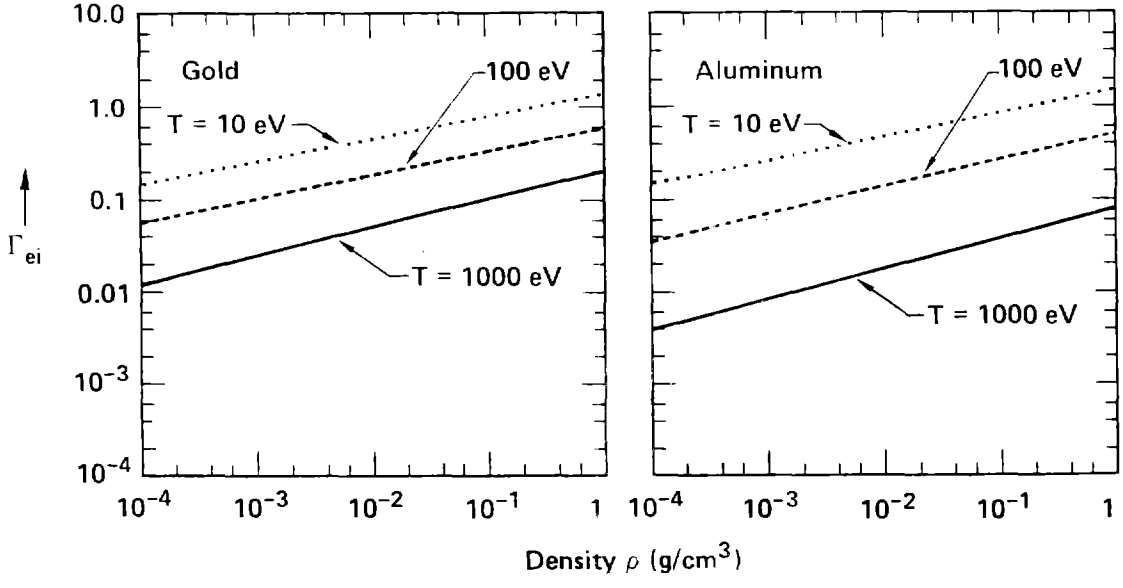

FIG. 11. Electron-ion coupling parameter Γ_{ei} for gold and aluminum plasmas. The small values illustrate rule G-4.

For materials other than hydrogen it is simplest to test the rule by examining numerical ionization data. Figure (11) shows $\Gamma_{ei}(\rho, T)$ calculated by the Thomas-Fermi cell model, accurate enough for present purposes; Γ_{ei} remains less than unity throughout the nondegenerate plasma range. At the lowest temperatures, Γ_{ei} approaches unity as one reaches solid density, but for degenerate electrons one should redefine Γ_{ei} using the Fermi energy rather than kT as a measure of electron kinetic energy; with this modified definition Γ_{ei} is again small at high pressures.

There is a logical reason for the general rule: if the attraction of ions for electrons strongly exceeds the electron kinetic energy, some electrons will recombine and the ion charge Q will decrease, reducing Γ_{ei}.

Electron-Electron Interaction

The interaction between free electrons is characterized by a coupling parameter Γ_{ee}^{free} which is smaller than Γ_{ei} by a further factor $Q^{2/3}$ (the 2/3 power reflects a corrected separation r_{12}). This means that $\Gamma_{ee}^{free} \ll 1$ and hence electron correlation effects are small, at least for free electrons.

Coulomb interactions between bound electrons are larger because the bound electrons are closer together. One can characterize these interactions by forming a bound-electron coupling parameter:

$$\Gamma_{ee}^{bound} = \frac{e^2}{r_n kT} \simeq \frac{I_n}{QkT} \sim \frac{\xi}{Q} \qquad (43)$$

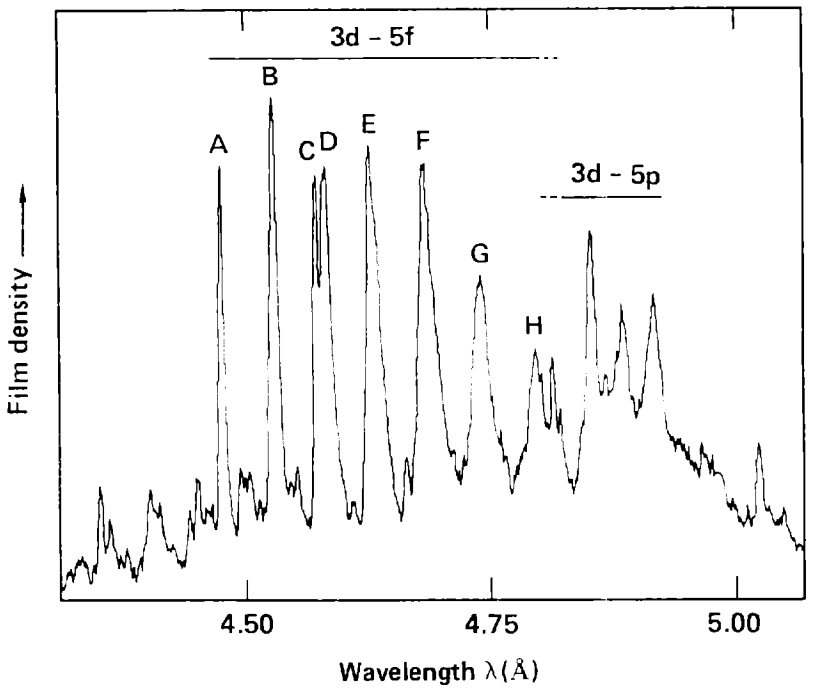

FIG. 12. Experimental spectrum of Ta plasmas illustrating sequence of UTA spectra (Andebert et al.[61]).

Evidently these interactions are often important (typical values of ξ and Q were given in Fig. 2). Electron interactions produce term splittings which are readily calculated for low-Z atoms or for ions carrying few bound electrons. For high-Z multielectron atoms the spectra become very complex and there is a nontrivial difficulty going beyond the one-electron (SCF or average-atom) approximation.

In recent years, statistical methods have been developed for the analysis of electron interactions in complex atoms. The term splitting for an arbitrary configuration is studied by moment expansion techniques by Bauche, Klapisch et al., a technique which is called the method of unresolved transition arrays (UTAs).[60] A representative recent application to analysis of laser-produced Ta spectra is given by Audebert, Gauthier et al. (Fig. 12).[61]

The distribution of configuration probabilities has been investigated through a high-temperature series expansion method (Green[62]), a technique which holds one population fixed and averages over occupations of other states (Grimaldi and Grimaldi-Lecourt[63]), and through direct numerical evaluation of configuration probabilities for a model Hamiltonian based on Eqs. (8-10).[2,3]

Figure 13 shows the complex spectrum of a gold plasma which is analyzed by identification of numerous specific transitions together with a schematized background from satellite configurations (Busquet, Pain, Bauche and Luc-Koenig[64]).

Degeneracy of Free Electrons

Qualitatively, an electron gas of density n_e is degenerate when the Fermi energy E_f,

$$E_f = \frac{\hbar^2}{2m} (3\pi^2 n_e)^{2/3} \tag{44}$$

exceeds the temperature kT ; this translates into a practical density criterion:

$$n_e \geq (1.4 \times 10^{23}/cm^3) \left(\frac{kT}{10\ eV}\right)^{3/2} \tag{45}$$

The criterion is usually satisfied for plasmas produced by shock compression of solid targets.

Degeneracy has a strong influence on plasma process coefficients, typically changing the form of their temperature-dependence. In many cases, the change amounts to replacement of the temperature by the Fermi temperature ($E_f = kT_f$), as in the electrical conductivity where a proportionality to $T^{3/2}$ is replaced by $T_f{}^{3/2}$. However, that rule is not general; the electron thermal conductivity in a non-degenerate plasma is proportional to $T^{5/2}$ and this is replaced by proportionality to $T \cdot T_f{}^{3/2}$.

Many theoretical treatments of plasma ionization incorrectly predict complete recombination at high densities.

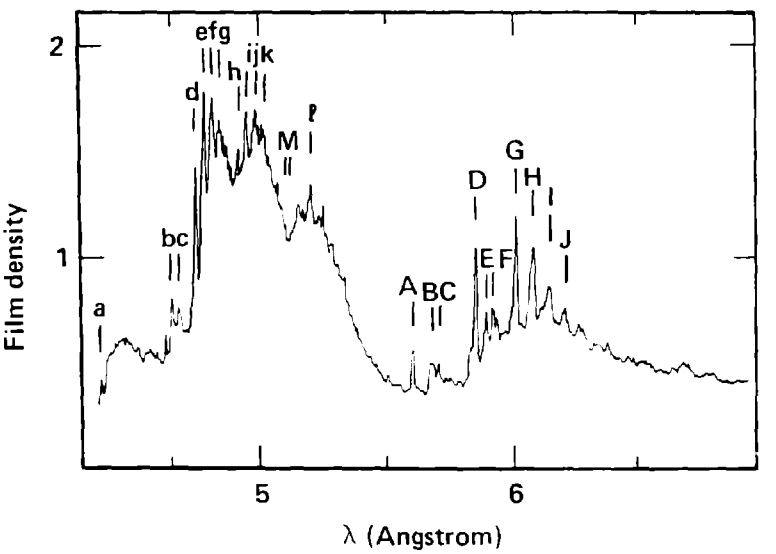

FIG. 13. Experimental spectrum of Au laser plasma illustrating complex line cluster features (Busquet et al.[64]).

For example, ionic rate equations employ an impact ionization rate proportional to $n_e n_i$ and a three-body recombination rate $\propto n_e^2 n_i$; with these rates the plasma recombines at high densities and cannot reach a degenerate state.[65]

What key ingredient must a theory include in order to handle the high-density degenerate case?

Degeneracy implies full (complete) occupation of all states having energies less than the Fermi energy E_f. Without pressure ionization there are an infinite number of bound states and these will absorb all Z electrons leaving no free electrons. Only if bound states are removed from the calculation by density effects will electrons be forced into free states to produce a degenerate free-electron gas.

This appears to be a general rule:

G-5.) Degeneracy of free electrons cannot occur without pressure ionization.

The rule applies to the construction of theories, not to nature. Experience with condensed matter leaves no question that both degeneracy and pressure-ionization occur at sufficiently high density in the real world.

At present one does not have a detailed configuration theory (i.e., Saha equation or ionic rate equation) which goes over to the high-density degenerate range in a satisfactory way. This difficulty of the Saha approach is one of the main unresolved questions of dense plasma theory.

The Saha equation (or ionic rate equations) are formulated in terms of exact energy-levels of the isolated ion. That is, the Hamiltonian is assumed to be diagonal when expressed in a basis of wave-functions in which bound electrons are localized on specific atoms (ions), or alternatively, many-body basis states in which each atom (ion) has an integral number of bound electrons.

However the Hamiltonian contains additional terms which are not diagonal in terms of basis states localized on individual atoms. Wave-functions $\psi_{n\ell}(r-R_i)$ centered on one ion overlap states $\psi_{n\ell}(r-R_j)$ centered on a neighbor ion, and this overlap leads to nonzero matrix-elements of kinetic and potential energy operators.

In low-density plasmas the off-diagonal hopping terms of the Hamiltonian are exponentially small, at least for states with small quantum numbers, but they rise with density. In the dense plasma the off-diagonal terms become very important. Alternatively, the charge on one ion is not a constant of the motion (even neglecting collisional or radiative processes which are treated as perturbations).

The upshot is that the Saha equation is untenable at high densities, and with it the entire language of hydrogen-like, helium-like ions (ion stages), ionization rate, etc.

Fortunately, the average-atom model remains workable at these conditions. The interatomic transfers associated with pressure-ionization are generated by one-electron operators (e.g., kinetic energy or central-field potential energy operators) and are readily incorporated in the average atom model. For this reason the average-atom theory yields results like the usual quantum theory of solids at high densities. Even the spherical-cell SCF model is accurate enough to agree with high-pressure shockwave data and appears to be essentially correct throughout the high-density degenerate range.(*)

To summarize,

G-5a.) Pressure ionization can be described in the AA model but not in the Saha theory. Alternatively, at very high densities, the AA is essentially correct.

It is not quite clear whether (G-5a) is a general rule or simply a generalization of recent experience. Hopefully the reader will be challenged to make his own judgement on this central question in the physics of dense plasmas.

(*) The problem with the average-atom model is that it does not exactly represent the electron-electron interaction, so that it predicts an incorrect line spectrum.

Excited States

Now we return to nondegenerate plasma conditions and examine the degree to which the highly-charged ion is susceptible to thermal excitation or perturbation by plasma microfields:

G-6.) The Z* theorem: at low densities, an ion is an isolated structureless point charge.

At low densities ($n_e < 10^{15}$ /cm^3) where this rule applies, one has little interest in atomic properties.[23] Ground-state ions are spatially separated by distances large compared to their size, scatter electrons like point charges and general behave in a simple fashion.

This behavior is a consequence of rule G-1: excitation energies are proportional to the ionization potential I(Z,Q) and at low densities become large in comparison with the temperature. Excited states therefore become exponentially improbable at low density.

This argument points the other way at high density where the key parameter ξ is not large (see Fig. 2):

G-6a.) At high density, all types of ionization (recombination) become rapid; ions are highly excited and no state persists long. Many plasma perturbations become strong but their effects overlap and average.

We give only a few examples here. In the complex spectra of high-density plasmas, satellite lines corresponding to multiply-excited ions are often prominent.[64] (See Fig. 13). Experimental spectra even understate this effect because the observed spectra usually come from nonequilibrium surface regions which typically have lower excited state populations than the bulk plasma

Second, we can compare rates for ion excitation or ionization with those for other electron-electron collisions. For example, the ratio of impact ionization to electron-electron scattering can be estimated using the Lotz formula:

$$\frac{\langle \sigma_{ii} v \rangle}{\langle \sigma_{ee} v \rangle} \sim \frac{1}{\xi^2} e^{-\xi} \qquad (46)$$

The result shows the rates become comparable when ξ becomes small. Another (related) estimate shows that the ion

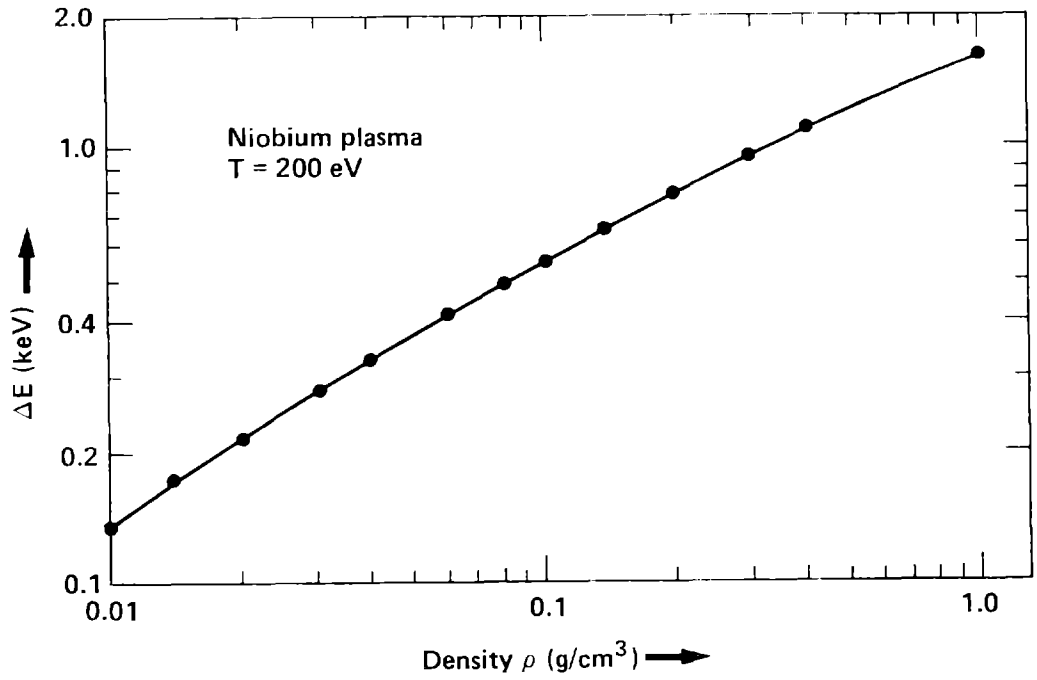

FIG. 14. Thermal average excitation energy per atom for Niobium plasma at various densities, calculated by solution of the Saha equation based on Eq. (10). As density rises the degree of excitation increases, illustrating rule G-6a.

scatters most electrons as a point charge when $\xi \gg 1$ but the quantum-mechanical form-factor or scattering amplitude becomes important when ξ becomes small.[2]

The comparison given in Eq. (46) is interesting because it bears on the possibility that a high rate of ionization might deplete the high-energy tail of the electron distribution more rapidly than electron-electron collisions can restore the Maxwellian form.

Third, one can examine the average excitation energy per atom for plasmas in thermal equilibrium (LTE). Figure (14) shows this excitation energy calculated by a Saha equation based on the screened hydrogenic model of Eqs. (8-10). The figure shows that excitation energy rises as density increases (for fixed temperature). For the case shown, the excitation energy reaches ~ 1 keV, enough to permit up to five autoionizations (for the typical ion) and the atomic internal heat capacity is comparable to the free electron specific heat.[3]

Rule G-5a enhances itself in the sense that the excited atoms (ions) existing at high densities are themselves more easily ionized, excited, polarized, etc. than groundstate ions would be.

Classical Behavior

It is a fundamental aspect of quantum statistics that all the exotic quantum phenomena (from superfluidity to the quantum hall effect) are demonstrated in cryogenic systems:

G-7.) Classical approximations become more accurate at high temperature, high density, high Z.

Our question here is a practical matter: can we determine the range of validity of Thomas-Fermi calculations, which are entirely classical except for including the exclusion principle in the form of the restriction

$$0 < f(r,p) < 1$$

for the one-electron distribution function.

The numbers given in Table II may help convince the reader that there is something to be explained: the statistical theory is in surprisingly close agreement with much more elaborate relativistic quantum-statistical calculations using both DCA and average-atom methods.

The TFD free energies have been supplemented with the Scott correction,[66] which is a constant in this case. The ACTEX (Activity expansion) theory[67] is based upon a Saha equation with elaborate summation of plasma corrections; it also employs the Planck-Larkin transformation, which helps explain the greatly increased charge state (see Table I). The INFERNO model is a spherical cell relativistic SCF theory.[41] The surprise is that the statistical model is within a few percent of the other theories.

Table II

Free energy F, entropy S and ionization state of Gold plasma at T = 630 eV and ρ = 10, 19.3, and 63 g/cm^3. F and TS are given in keV per atom.

	TFD	ACTEX	INFERNO	MAXIMUM DIFFERENCE
F	639	654	653	2.3%
TS	214	-	210	1.9%
Z*	42.8	48.9	42.6	
F	622	638	637	2.6%
TS	190	-	187	1.6%
Z*	39.6	48.3	40.9	
F	595	-	611	2.7%
TS	151	-	148	2.0%
Z*	37.9	-	38.5	

The general assertion that classical statistics becomes correct at high temperature must confront the pronounced quantum effect of K-shell ionization, visible in any quantum ionization calculation. Is there a definite mathematical theorem underlying rule G-7?

One precise statement of the general rule is obtained from the quantum density matrix $\rho(r, r')$ of a nondegenerate free electron in volume V:

$$\rho(\underline{r},\underline{r}') \equiv (\underline{r}|\frac{1}{Z}e^{-\beta H}|\underline{r}')$$

$$= \frac{1}{V} \exp - [\pi(\underline{r} - \underline{r}')^2/\lambda]^2 \qquad (47)$$

Here Z = Trace $[\exp(-\beta H)]$ = partition function; $H = p^2/2m$ = free electron Hamiltonian, and $\lambda = (2\pi\hbar^2/m_e kT)^{1/2}$ = thermal deBroglie wavelength.[68] This expression reduces to the diagonal (=classical) form as $T \to \infty$.

Equation (47) says that quantum effects can only occur on a small size-scale $\leq \lambda$, i.e., only for the innermost bound electrons at high temperature. The remaining electrons are therefore adequately described by the classical (statistical) theory.

A similar (inequivalent) result is the observation that the exchange energy per electron,

$$f_{exch} = \frac{1}{12} \frac{e^2}{\lambda} (n_e\lambda^3) \qquad (48)$$

becomes small as $T \to \infty$; of course the exchange energy is a quantum correction to the classical TF theory.

For dense plasmas the high thermal excitation indicated by rule G-6a tells us that the effects of various quantum states will be averaged or smoothed leaving only continuous (i.e., classical) behavior.

Figure 15 compares ionization states $Z^*(T)$ for aluminum and gold plasmas at constant density $\rho = 10^{-3}$ g/cm^3 calculated by the screened hydrogenic model (which includes quantum shell effects) and the Thomas-Fermi theory.[2] The comparison shows the TF approximation to be more accurate at high Z. Figure 16 shows a perspective drawing of $Z^*(\rho,T)$ for aluminum. In this case the figure shows the quantum ionization shelf-structure, associated with the helium-like ion, disappearing at higher densities.

Active Particles

The next "general rule" poses problems: we are not certain it is a rule, nor what would be the proof. However it summarizes a variety of situations, and has proven useful in detecting errors in complex calculations -- and that is the acid test of utility. The statement is simple enough:

G-8.) A small number of high-energy particles can easily dominate the properties of an equilibrium plasma. A small number of low-energy (inactive) particles cannot.

The obvious example is electrical: a few ions in a neutral gas can easily dominate the conductivity; a few neutrals in a strongly ionized gas have little effect.

In the calculation of thermal conduction by electrons or radiation it emerges that the net heat current is strongly dominated by a small minority of electrons (or photons) at the high-energy tail of the distribution. In these cases the reason is the rapid increase of mean free path with energy. Ionization is also dominated by the most energetic particles, as rule G-1 implies.

Other examples of active particles are the suprathermal electrons produced in laser-plasma interaction, and high energy x-rays they produce through bremsstrahlung or K-shell ionization and fluorescence. These have great importance as preheat sources, even when they carry as little as a few percent of the absorbed energy.

In thermonuclear plasmas it is not unusual to find the fusion rate dominated by collisions involving energetic ions in the hot tail of the distribution. For this reason, the processes involving these energetic ions (energy loss, escape, energy transfer to knock-on particles) assume special importance.

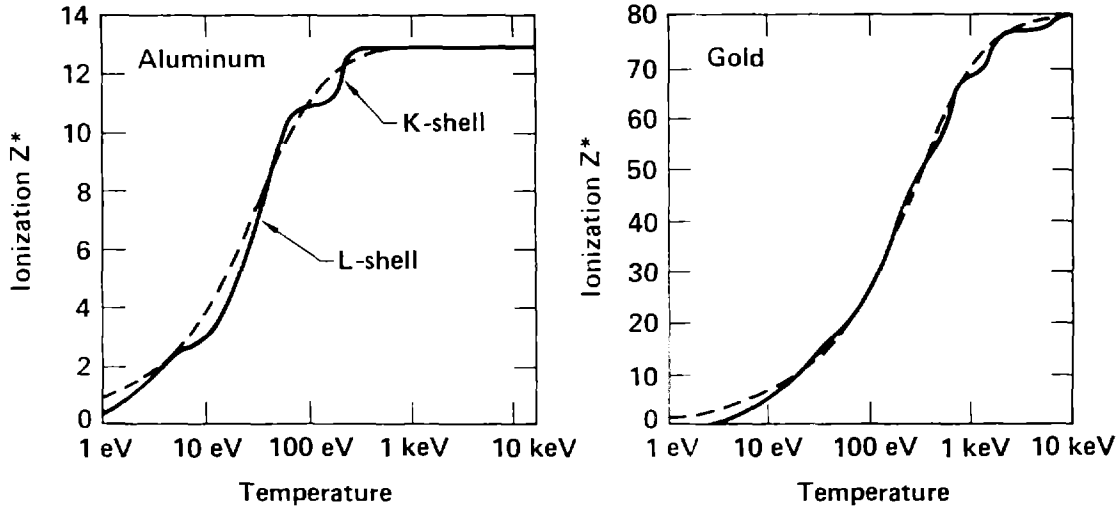

FIG. 15. Ionization state of Aluminum and Gold at density 10^{-3} g/cm^3. Solid line is the screened hydrogenic average-atom model. Dashed line is the Thomas-Fermi theory. The two approaches are in closer agreement for the larger Z, illustrating rule G-7.

A nice example of rule G-8 is given in the Appendix. There it is shown that the few bound electrons cannot dominate the stopping-power, e.g., for fast alphas resulting from thermonuclear reactions, even under the special conditions

$$v_{Bohr} \ll v_{ion} \ll v_e = (kT_e/m_e)^{1/2}$$

where the free-electron stopping is inhibited by a large factor $(v_{ion}/v_e)^3 \ll 1$. One would reach an incorrect conclusion in this case without include the process of pressure ionization.

Another (related) example is that the large photoelectric cross-section of bound electrons cannot dominate the opacity of a mostly-ionized equilibrium plasma (again, the proposition refers to the case of high temperatures at which most ions are fully stripped, so bound electrons are indeed a minority).

The rule is not perfectly general, as we have seen from interesting counterexamples given in the lectures of Dalgarno; neutral hydrogen injected into highly-ionized plasma produces distinctive and dominant radiative emission via charge-transfer.[69] Of course there would be very little neutral hydrogen in these plasmas if they were closer to thermal equilibrium.

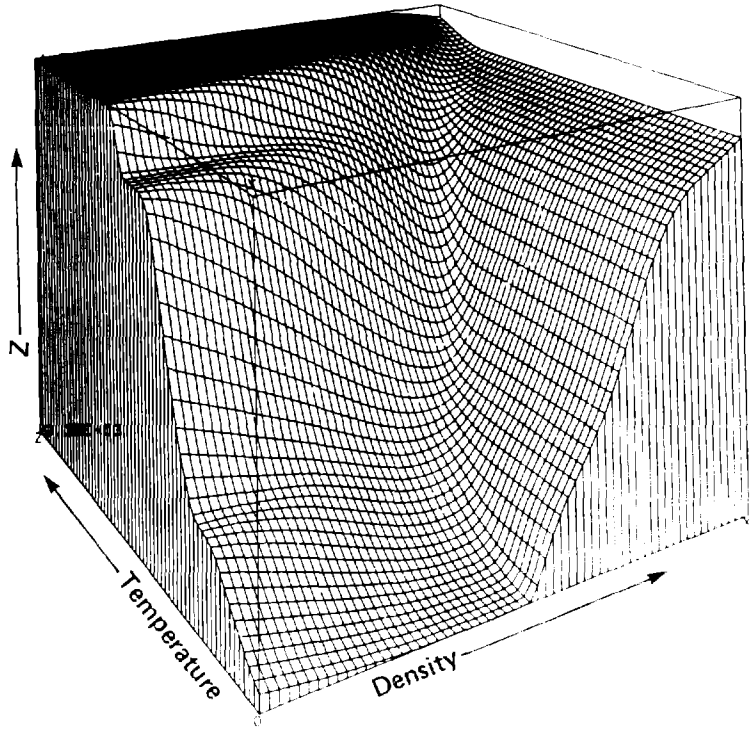

FIG. 16. Contour plot of Aluminum ionization state calculated by the screened hydrogenic model of reference 17. The density range is 10^{-4} to 10^{+4} g/cm^3; the temperature range is 10 eV to 10^4 eV. Note (1.) Pressure ionization at high densities, (2.) reduced prominence of the K-shell ionization plateau as density rises. This illustrates rule G-7.

V. INTERCONNECTION OF PLASMA PROCESSES

As a target is irradiated by laser or particle beam, the absorbed beam energy is transferred into electron, ion and photon distributions and ultimately appears as kinetic energy of hydrodynamic motion, emitted x-rays, magnetic fields, etc. These energy conversions are described by plasma process coefficients: rate coefficients which enter equations describing the macroscopic plasma hydrodynamics. For example, the specific heat and pressure measure the conversion of absorbed energy into temperature and hydrodynamic motion, the stopping power dE/dx tells how ion (or electron) beam energy is deposited, the coupling τ_{ei} describes heat exchange between electrons and ions, and the opacity κ_ν determines the x-ray mean free path $\ell_\nu = 1/\rho\kappa_\nu$.

The plasma process coefficients reflect atomic events including scattering, ionization and bound-electron transitions as they occur in the dense plasma environment. The rates are functions of plasma composition, density and temperature and/or state of nonequilibrium. The practical

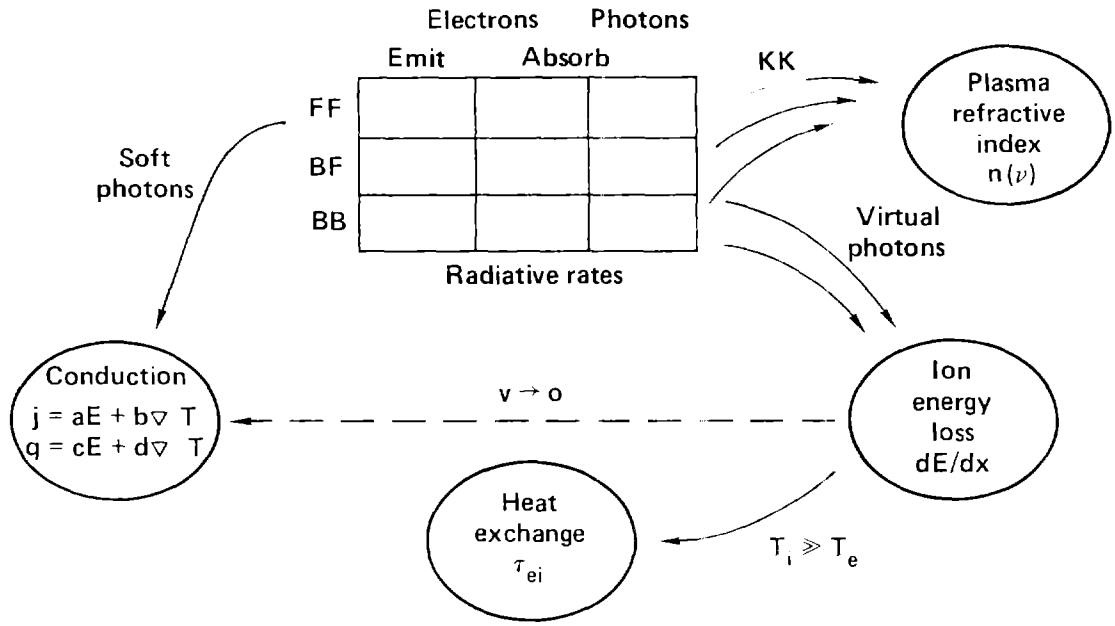

FIG. 17. Schematic illustration of rule G-11. The rectangular box represents radiation formulas corresponding to free-free (FF), bound-free (BF) and bound-bound (BB) emission or absorption processes. The absorption formulas can be written as electron or photon cross-sections. These processes are related by detailed balance and continuity in energy. The soft photon ($h\nu \to 0$) limit of the FF cross-section is equivalent to the electrical conductivity. The plasma index $n(\nu)$ is obtained by Kramers-Kronig transformation of the photon absorption cross-section, and the fast-ion stopping dE/dx equivalent to absorption of virtual photons. The heat-exchange between electrons and ions is an average of dE/dx in the special case $T_i >> T_e$ and finally the low-velocity ion stopping is given by a friction coefficient related to the electrical conductivity.

output of theory is measured by our ability to predict the process coefficients. The discussion in this section will emphasize three general rules,

---

G-9.) Observable plasma properties change continuously as bound states convert into free states.

G-10.) Detailed balance: each process rate is related by time-reversal to the rate for the inverse process.

G-11.) The plasma process coefficients are linked together by a network of exact and/or qualitative consistency relations.

The rules are illustrated throughout the following. One example of rule G-11 is the consistency of pressure $p(\rho, T)$ and energy $E(\rho, T)$; for equilibrium plasmas this is a simple thermodynamic equation, but for nonequilibrium plasmas it developes into an extension of conventional statistical mechanics (More[3], Boercker and More[70]). Another example is the Kramers-Kronig relation between plasma refractive index $n(\nu)$ and the absorption opacity κ_ν.[71,72] These are exact connections.

A qualitative consistency must exist between opacity and the charged-particle stopping-power: dE/dx is essentially a mean opacity analogous to the Planck or Rosseland means, i.e., a certain average of the photon absorption cross-section. This connection is seen by representing the electromagnetic field of a fast charged particle as a superposition of virtual photons having the frequency distribution:

$$N(h\nu) \simeq \frac{2\alpha}{\pi h\nu} Q^2 \left(\frac{c}{v}\right)^2 \log\left(\frac{av^2}{b_o h\nu}\right) \qquad (49)$$

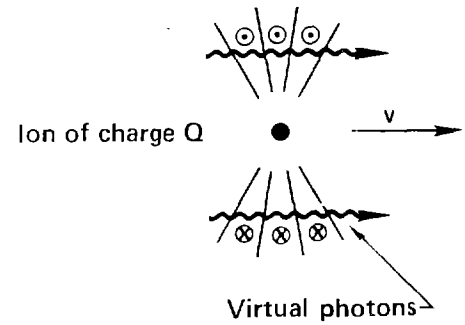

FIG. 18. A fast ion is surrounded by electric and magnetic fields which are approximately equivalent to a cloud of comoving photons.

In this well-known expression v = ion speed (assumed $\ll$ c), c = speed of light, $\alpha = e^2/\hbar c$ = fine-structure constant, a = constant ~1 and b_o = minimum impact parameter.[72]

The charged-particle energy-loss results from absorption of these virtual photons by bound or free electrons of the target plasma. Strictly speaking, virtual photons do not obey the dispersion relation $\omega = c\,k$ of free photons, but this does not matter to the extent that one uses the dipole approximation in the absorption calculation. The bound-bound absorption opacity generates an energy-loss of the form:

$$-\left(\frac{dE}{dx}\right)_{BB} = \int h\nu\, N(h\nu)\, \rho\kappa_\nu^{BB}\, dh\nu \qquad (50)$$

$$= \frac{4\pi Q^2 e^4}{mv^2}\, n_I \sum_{n,m} f_{nm}^{abs}\, P_n \left(1 - \frac{P_m}{D_m}\right) \log\left(\frac{av^2}{b_o h\nu_{nm}}\right)$$

This expression looks like the bound electron contribution to the Bethe (high-velocity) stopping theory when the appropriate minimum impact parameter $b_o = \hbar/mv$ is selected.

In the Bethe theory, bound-bound (line) and bound-free (photoelectric) transitions together are represented by the expression

$$\left(\frac{dE}{dx}\right)_{bound} = \frac{4\pi Q^2 e^4}{mv^2}\, n_I \log\left(\frac{2mv^2}{\bar{I}(Z,Q)}\right) \qquad (51)$$

where $\bar{I}(Z,Q)$ is a logarithmic mean of excitation and ionization energies as indicated by Eg. (50). There is also a free electron contribution, calculated by Skupsky and Deutsch,[73,74] which has a similar analytic form in which $\bar{I}$ is replaced by $\hbar\omega_{pe}$, the electron plasma frequency of free electrons, in the high-velocity case. For a practical stopping formula, one therefore requires a convenient representation of the bound-electron contribution, i.e., $\bar{I}(Z,Q)$.

This quantity has been calculated by Thomas-Fermi theory using arguments based on the inhomogeneous electron-gas model, closely related to the original Bloch theory.[3,75] The Thomas-Fermi calculations are accurately reproduced by

$$\bar{I} = a\, Z\, \frac{\exp\left[1.29x^{.72} - .18x\right]}{\sqrt{1 - x}} \qquad x = Q/Z \qquad (52)$$

The coefficient a is $\simeq$ 10 eV. With this formula one obtains a simple and useful description of the high-velocity stopping power of partially-stripped nondegenerate plasmas. Figure 19 compares Eq. (52) with quantum calculations performed by E. McGuire.[76]

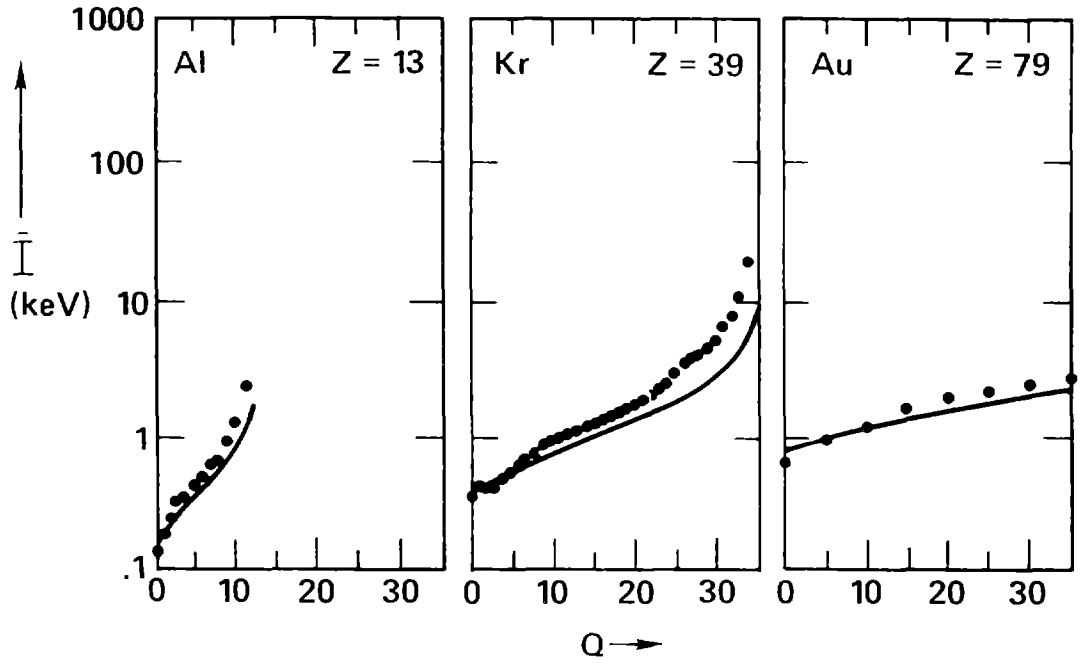

FIG. 19. The mean ionization-excitation potential $\bar{I}(Z,Q)$ for ions of Al, Kr and Au. Solid line is the TF result, Eq. (52). Dots are results from quantum generalized oscillator-strength calculations kindly provided by Dr. E. McGuire.[76]

Another example of rule G-11: the collisional electron-ion heat exchange coefficient of Eqs. (19-20) can be calculated from the stopping power because in the special case $T_i \gg T_e$ the heat transfer is the same process as fast-ion energy-loss to the cooler electrons. In this case, however, we use the energy-loss expression valid for $v_e \geq v_i$ (this is the free-electron contribution in Eq. (A-10)), and average over the ion Maxwell distribution,

$$\frac{1}{\tau_{ei}} = \frac{1}{T_i}\frac{dT_i}{dt} = \frac{1}{\frac{3}{2}n_i k T_i}\left\langle v_i \frac{dE_i}{dx}\right\rangle \qquad (53)$$

With the proper choice of Coulomb logarithm, the result is the Landau-Spitzer heat-exchange time (see Eqs. (19, 20) above).

These examples illustrate the utility of the connections between plasma processes: if we encounter a dense-plasma mechanism which alters the photon absorption opacity, Eqs. (50, 53) will suggest related improvements in the formulas for stopping power and electron-ion coupling τ_{ei}.

Rule G-10 belongs to the general structure of statistical mechanics; it plays a powerful role in developing consistent descriptions of the plasma processes. For example, it relates absorption and emission cross-sections. Another typical application was given in section II.

Rule G-9 concerns the continuum and bound states near it. In general terms, the uppermost bound states have much

in common with the continuum states. In a more precise sense there are three related ideas: correspondence, analyticity in energy and the continuity of bound and free states.

The correspondence principle of the old quantum theory is the idea that a classically defined quantity q_n (e.g., orbital frequency or radiation emission rate) approaches the classical value at large quantum number n:

$$\lim_{n \to \infty} q_n^{QM} = q_n^{Classical} \tag{54}$$

The principle was originally formulated for hydrogenic spectra which have infinitely many bound states, so that the limit $n \to \infty$ is defined. From the quantum viewpoint, the correspondence principle is simply the fact that the WKB approximation becomes reasonably accurate at large quantum numbers (but is not exact in general).

The analytic connection between bound and free states is illustrated by the well-known result that bound-electron eigenvalues $E_{n\ell}$ are poles of the continuum scattering or S-matrix $S_\ell(E) = e^{2i\delta_\ell(E)}$, or by the formula of Seaton[77] which relates quantum defects $\Delta_{n\ell}$ (for large quantum number n) to the low-energy scattering phase-shifts $\delta_\ell(E)$.

These are connections of negative-energy and positive-energy solutions of the Schroedinger equation, proven by extrapolation or analytic continuation in energy. They are rigorous results of the one-electron theory and in most cases apply to any potential V(r), although they may require modification for long-range potentials.

The continuity principle states that observable plasma properties including the energy per particle, the pressure and opacity coefficients are continuous functions of density even at those special densities $\rho_{n\ell}$ where a bound state is pressure-ionized into the continuum. Likewise, the properties are continuous functions of nuclear charge Z.

These continuity principles have an interesting history.[44,78] As with many of the general rules, they provide a way to identify incorrect or unsatisfactory physical models. They also give powerful guidance in developing approximate formulas for bound electrons. One example is the Burgess-Merts formula for dielectronic recombination, obtained by extrapolating an impact-excitation cross-section to energy transfers where the incident electron is captured.[79] However the classic application of the continuity principle is the work of Kramers which we review and extend in this section.

Kramers' Hydrogenic Radiation Formulas

The emission of x-rays by free-free (FF), free-bound (FB) and bound-bound (BB) processes in a plasma are

described by the following kinetic equations, which give the number of photons emitted per cm^3-sec-keV:

$$\frac{dN^{FF}}{d^3r\ dt\ dh\nu} = n_I \int \frac{2d^3p_o}{h^3} |v_o|\ f(\epsilon_o)\frac{d\sigma^{Bremss}}{dh\nu}\ (n_\nu+1)[1-f(E)] \quad (55)$$

$$\frac{dN^{FB}}{d^3r\ dt\ dh\nu} = n_I \sum_n \int \frac{2d^3p_o}{h^3} |v_o|\ f(\epsilon_o)\frac{d\sigma^{FB}}{dh\nu}\ (n_\nu+1)[1-\frac{P_n}{D_n}] \quad (56)$$

$$\frac{dN^{BB}}{d^3r\ dt\ dh\nu} = n_I \sum_n \sum_{no} P_{n_o}\ A_{n_o \to n}\ (n_\nu+1)[1-\frac{P_n}{D_n}] \quad (57)$$

In these equations, n_I = number density of target ions, $f(\epsilon_o)$ = distribution function for incident free electrons, n_ν = number of photons per mode at energy h_ν, P_n = population of bound-states in shell of principal quantum number n and $A_{n_o \to n}$ = Einstein rate coefficient, $p_o = m\ v_o$ = momentum of incident electron. The degeneracy factor $[1 - f(\epsilon)]$ or $[1 - Pn/Dn]$ describes possible occupation of the final state.

The Kramers cross-sections are:[13,80]

$$\frac{d\sigma^{Bremss}}{dh\nu} = \frac{8\pi}{3\sqrt{3}}\ \frac{Z^2\alpha^3a_o^2}{h\nu}\ (\frac{e^2/a_o}{\epsilon_o}) \quad (58)$$

$$\frac{d\sigma^{FB}}{dh\nu} = \frac{8\pi}{3\sqrt{3}}\ \frac{Z^4\alpha^3a_o^2}{n^3}\ (\frac{e^2/a_o}{\epsilon_o})\ (\frac{e^2/a_o}{h\nu})\ \delta(\epsilon_o - h\nu - E_n) \quad (59)$$

$$A_{n_o \to n} = \frac{8\pi^2e^2\nu^2}{mc^3}\ f^{emiss}_{n_o,n}\ I(h\nu) \quad (60)$$

where the line profile $I(h\nu)$ and emission oscillator-strength obey

$$\int_{-\infty}^{\infty} I(h\nu)\ dh\nu = 1 \quad (61)$$

$$f^{emiss}_{n_o,n} = \frac{n^2}{n_o^2}\ f^{abs}_{n,n_o} = \frac{n^2}{n_o^2}\ \frac{32}{3\pi\sqrt{3}}\ \frac{n\ n_o^3}{(n_o^2 - n^2)^3} \quad (62)$$

The Kramers bremsstrahlung emission cross-section is derived from classical radiation theory: a free electron of energy $\epsilon_o = 1/2m\ v_o^2 > 0$ approaches a point nucleus of charge + Ze along a hyperbolic trajectory. The electron gains a kinetic energy $\simeq Ze^2 / r_{min}$ as it approaches its innermost radius $r_{min} \simeq a_o\ell^2/Z$ ($\hbar\ell$ is the angular

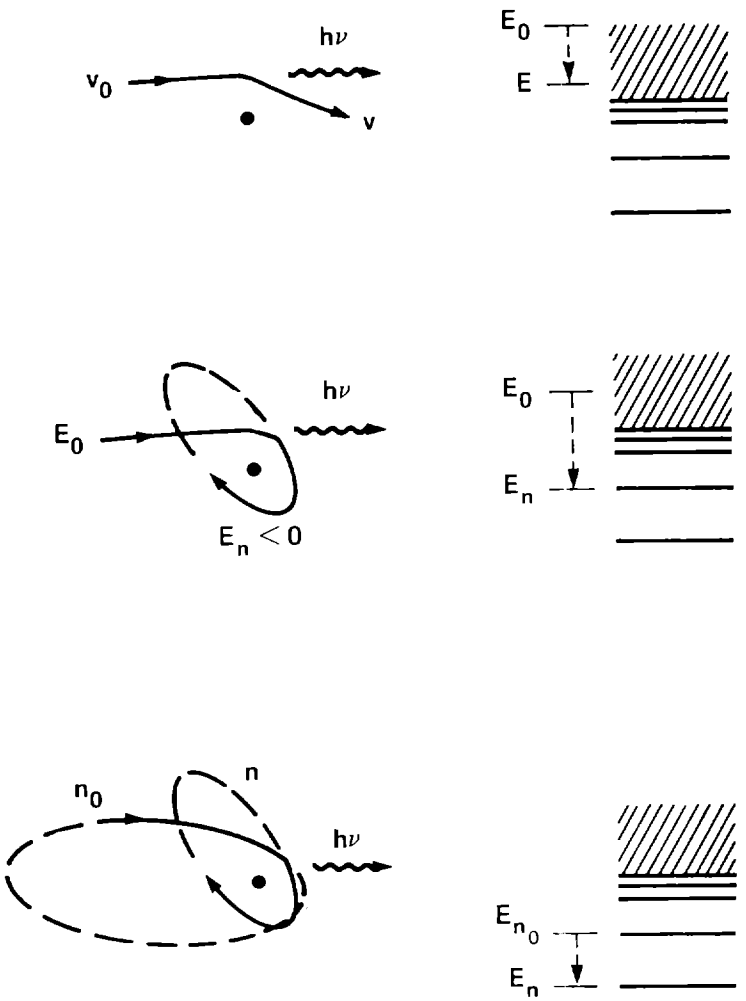

FIG. 20. Schematic representation of free-free, free-bound and bound-bound emission processes. The formulas which describe these processes are closely related because the emission occurs during the strong acceleration near the target nucleus.

momentum). For the collisions which produce the majority of the emission, r_{min} is small; Kramers' calculation is most accurate for the case where $Ze^2 / r_{min} \gg \epsilon_0$. The opposite limit is described by the Born approximation. In the Kramers case, the electron follows a hyperbolic path with strong curvature; the closest portion of the orbit is at radius $\sim r_{min}$ and is traversed at velocity

$v_{max} \approx \sqrt{\frac{2mZe^2}{r_{min}}}$ giving radiation of frequency $\lesssim \frac{r_{min}^{3/2}}{\sqrt{2mZe^2}}$.

The radiated energy spectrum is calculated by fourier analysis of the acceleration and then summed over impact parameters (angular momenta); the result is Eq. (58).[81]

We emphasize that this calculation describes the classical non-relativistic bremsstrahlung of an electron colliding with an isolated point charge. There are many physical corrections:

a.) Even for collisions with a point charge ion, the quantum theory gives a correction referred to as the Gaunt factor.[82]

b.) For collisions with a high-Z point charge there are significant relativistic corrections. These corrections can be appreciable even for $\epsilon_o \ll mc^2$ if the kinetic energy $\approx Ze^2 / r_{min}$ is relativistic.

c.) For collisions with partially-stripped ions, the emission cross-section is likely to vary between a Kramers cross-section determined by the ion charge Q for soft photons to that determined by the nuclear charge Z for hard photons produced at small radii. This bound-electron screening correction is discussed by Lamoureux and Pratt[83] and Kogan and Kukushkin.[84]

Numerical calculations of bremsstrahlung from partially stripped ions including effects (a,b,c) are reported by Feng and Pratt,[85] Lee and Pratt.[86]

d.) One dense-plasma effect is plasma degeneracy, represented by the final-state factor [1-f] in Eq. (5). In the Kramers approximation the effect of degeneracy on the net emission rate turns out to have simple analytic form.[2,87]

e.) In dense plasmas, the plasma dielectric function alters the dispersion relation of the outgoing photon. This effect is interesting because it alters the detailed-balance equations, but the results are not quantitatively large in typical laboratory plasmas.[88]

f.) Another dense-plasma effect is screening of the ion potential by the exterior plasma. This has been calculated analytically by use of the Born approximation for the scattering;[89] however the Born approximation is very inaccurate in the case of greatest practical interest (the Kramers case mentioned above).[90,91] In reality, most of the radiated photons originate at small radii where plasma screening is not large.[92]

g.) A more sophisticated calculation of the screening effect describes the environment with ion pair-correlation functions.[93] The result is interference between scattering by adjacent ions. This calculation is also limited to the Born approximation and produces its main effect for low-energy electrons (for which the Born approximation is surely invalid).

h.) In practice there is considerable interest in the possibility of significantly non-Maxwellian electron distributions in laser-plasma experiments. The predicted changes in bremsstrahlung spectrum, following from Eq. (5), are quite substantial and may help identify non-Maxwellian distributions in experimental continuum emission spectra (Lamoureux, Moller and Jaegle[94]).

Of these corrections to the Kramers' formula for bremsstrahlung, we will focus on the largest: the question of effective charges which replace the nuclear charge Z when the plasma is not fully ionized. Normally recombination and line emission are strongly dominant in a partially-ionized plasma; exactly the same question of effective charges arises for those processes. We will examine Kramers' connection of bremsstrahlung, recombination and line emission in order to derive modified Kramers formulas which apply to partially-stripped ions.

To calculate radiative recombination, Kramers extrapolates the bremsstrahlung emission cross-section of Eq. (58) to events in which $h\nu > \epsilon_o$. All transitions to energies near the quantized final energy E_n are grouped together as

$$\frac{d\sigma^{FB}}{dh\nu} = \frac{d\sigma^{Bremss}}{dh\nu} \frac{\partial E_n}{\partial n} \delta(\epsilon_o - h\nu - E_n) \qquad (63)$$

For hydrogenic ions, $E_n = - Z^2 e^2/2a_o n^2$ and this equation correctly connects Eqs. (58, 59). For ions with bound electrons we employ Eq. (8) for the eigenvalue E_n, with a level spacing

$$\frac{\partial E_n}{\partial n} \simeq \frac{Q_n^2 e^2}{a_o n^3}$$

For recombination into shell n it is natural to assume the effective charge Q_n enters the extrapolated bremsstrahlung cross section; this is because the radiation occurs close to the inner turning point. With these assumptions Eq. (63) gives a nonhydrogenic cross-section (we omit the energy-conserving delta-function):

$$\sigma^{RR}(\epsilon_o) = \frac{8\pi}{3\sqrt{3}} \frac{Q_n^2 a_o^2 \alpha^3}{h\nu} \left(\frac{e^2/a_o}{\epsilon_o}\right) \frac{\partial E_n}{\partial n} \qquad (64)$$

$$\propto Q_n^4 / (n^3 \epsilon_o h\nu)$$

This expression has been extensively compared to more elaborate quantum calculations and gives very satisfactory agreement. One example of these comparisons is reported by Huebner, Argo and Ohlsen.[95] To obtain good agreement, it is essential that an inner-screening effective charge be employed in Eq. (64).

Next we examine the case of line emission. In order to treat this as a continuation of radiative recombination we employ a special trick, one which has a very pleasing intuitive content. The idea is to regard the upper electron's interaction with the nuclear potential as a collision. Because the radiative transition happens during the strong acceleration occuring close to the nucleus, we can imagine that it is not important whether the asymptotic energy is

positive ($\epsilon_o > 0$) or negative ($E_{n_o} < 0$).

We assume there are P_{n_o} electrons in the upper level n_o, statistically distributed over the subshell states, so that

$$P_{n_o,\ell} = 2(2\ell + 1)(P_{n_o}/2n_o^2)$$

The electrons in states of small angular momenta (elliptical orbits) approach the nucleus with the orbital frequency $\nu_{n_o} = (1/h)(\partial E_{n_o}/\partial n_o)$ giving a collision rate:

$$\frac{dN_\ell}{dt} = P_{n_o,\ell}\ \nu_{n_o} \tag{65}$$

Now we define an effective incident electron flux,

$$\Phi_{n_o} = \left(\frac{P_{n_o}}{2n_o^2}\right) \frac{2m|E_{n_o}|}{\pi^2\hbar^2} \quad \frac{1}{\hbar} \frac{\partial E_{n_o}}{\partial n_o} \tag{65}$$

If the idea of a uniform incident flux makes sense, then a geometrical calculation of the collision rate should agree with Eq. (65). With an impact parameter b determined by $mv_{n_o}b = \hbar(\ell + 1/2)$ the geometric calculation is

$$\frac{dN_\ell}{dt} = \Phi_{n_o}\ 2\pi b\ db \tag{67}$$

One readily verifies that this agrees with Eq. (65).

To summarize: the bound electron(s) in state n_o are equivalent to a uniform incident flux Φ_{n_o} in terms of the rate of close approaches to the nucleus. With this equivalence, the line emission rate is a straightforward extrapolation of the radiative recombination rate of Eq. (56),

$$\frac{dN^{BB}}{d^3r\ dt\ dh\nu} = n_I\ \Phi_{n_o} \frac{d\sigma^{BB}}{dh\nu} (n_\nu + 1)[1-P_n/D_n] \tag{68}$$

with the formal extrapolation

$$\frac{d\sigma^{BB}}{dh\nu} = \frac{d\sigma^{FB}}{dh\nu} \tag{69}$$

Again the charge Q appearing explicitly is replaced by the effective charge Q_n of the lower state on the grounds that the acceleration occurs at small radii.

This reasoning gives

$$\frac{d\sigma^{BB}}{dh\nu} = \frac{8\pi}{3\sqrt{3}} \frac{\alpha^3 a_o^2}{h\nu} (Q_n^2 \frac{dE_n}{dn})(\frac{e^2/a_o}{E_{n_o}})\ \delta(E_{n_o} - h\nu - E_n)$$

When Eq. (68) is forced back into the usual form of Eq. (60) we find an expression for non-hydrogenic oscillator strengths,[2]

$$f^{abs}_{n\to n_o} = \frac{4}{3\pi\sqrt{3}} \left(\frac{e^2/a_o}{h\nu}\right)^3 \frac{Q_n^4\, Q_{n_o}^2}{n^5\, n_o^3} \tag{70}$$

Equation (70) gives a remarkably simple prediction of shell-averaged oscillator-strengths for arbitrarily charged ions.

From the derivation it is obvious that Eq. (70) reduces to the hydrogenic form of Eq. (62) whenever $Q_n = Q_{n_o}$. Of course Eq. (62) is not exact for hydrogenic ions; there are relativistic and quantum corrections of the order of 50 % (Bethe and Salpeter,[96] Rose[97]).

However Eq. (70) manages to nicely reproduce the largest effect of screening (Fig. 21). In the example shown, certain oscillator-strengths change by as much as a factor ~ 10 during ionization and Eq. (70) follows this dependence to ~ 50 % accuracy.

Eq. (70) explains a semi-empirical scaling law for 1s-np transitions recently observed by Benka and Watson.[98]

The physical content of Eq. (70) has been recognized by many previous workers: the dominance of the effective charge of the innermost turning point and the factors $\partial E_n/\partial n$ which which are equivalent to wave-function normalization factors. It is also true that more accurate oscillator-strengths are readily obtained from quantum calculations. However Eq. (70) represents a significant advance for applications in which a high priority is placed upon simplicity and generality.

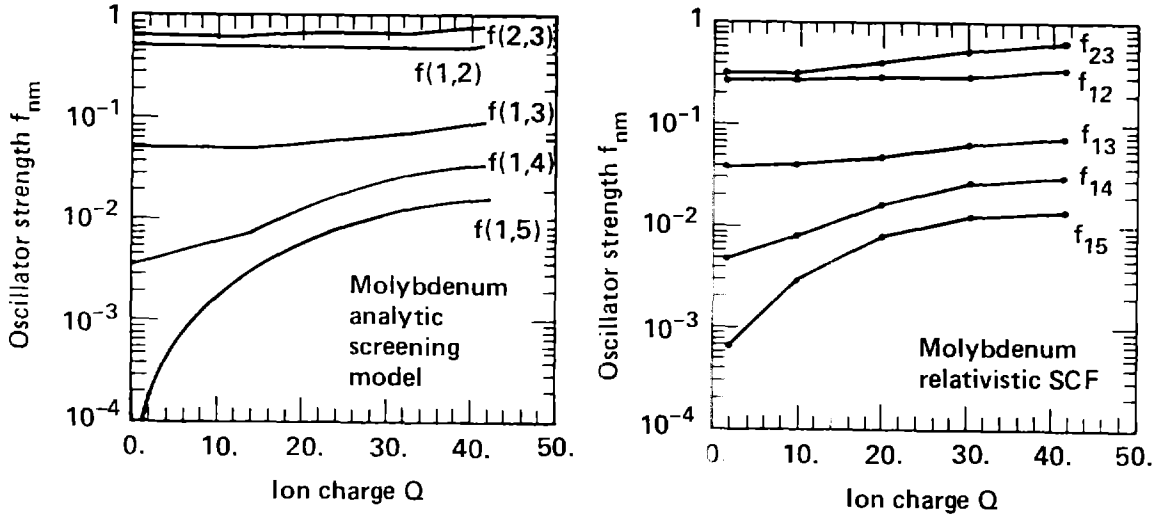

FIG. 21a, 21b. Absorption oscillator-strengths for Molybdenum ions. $f_{nn'}$ is averaged over initial states and summed over final states. The analytic screening model consists of Eq. (70) evaluated with the screening coefficients of reference 18. The relativistic SCF calculations were performed by D. A. Liberman.

Reverting to the broader perspective of this section, it is useful to reconsider Eqs. (63) and (69). These equations have shown how to convert the formulas for brems- strahlung into expressions for recombination and line emission. The point of greatest interest is that when we calculate radiative processes including various density effects, some version of these connection formulas should remain valid. This will provide powerful guidance toward the future development of a complete understanding of high-density plasma radiative phenomena.

VI. NONEQUILIBRIUM PHENOMENA

We conclude this survey with a few comments on non-equilibrium (NLTE) phenomena.

If we consider high-density nonequilibrium plasmas there are two simplifications: first, at high enough density our equations will predict LTE conditions; for each ionization or excitation process, according to rule G-10, forward and reverse rates cancel in (or near) LTE. This reduces the number of independent cross- sections and also points to reduced sensitivity to approximations in the rates.

Second, many density effects are essentially the same for LTE or non-LTE plasma conditions. For example, Coulomb interactions affect the classical motion of point-like ions, independent of the radiation spectrum or bound-electron excitation state; the resulting pair-correlation is the same in LTE or non-LTE cases. Likewise the phenomena of pressure ionization should be very similar in LTE, NLTE cases.

These remarks indicate that non-LTE plasmas are not entirely unlike the LTE plasmas considered so far.

NLTE in Laser Experiments

How is NLTE observed experimentally? The answer is indirect: experimental spectra are compared to elaborate computer simulations of laser target hydrodynamics including energy transport, ionization, and x-ray production with special treatment of nonequilibrium electron, photon and ion distributions. Calculations performed with LTE and non-LTE ionization assumptions differ dramatically.

Rosen et al.,[99] compare theoretical and experimental spectra for gold disk targets irradiated at 3.10^{14} W/cm^2 (λ = 1.06μ). The LTE calculation predicts 2-3 keV line emission which is ~ 100 times stronger than either crystal spectrometer data (confirmed by filtered XRDs) or the NLTE calculation. This enormous difference is due to the plasma ionization state: the NLTE calculation predicts lower ion charges and emission of softer photons.

The comparison of simulation and experiment is neither simple nor direct because the computer calculation inevitably involves ad hoc prescriptions for several key aspects of the physics, including laser absorption mechanisms, magnetic field generation and inhibited electron thermal conduction. The non-LTE calculations are also relatively crude, using

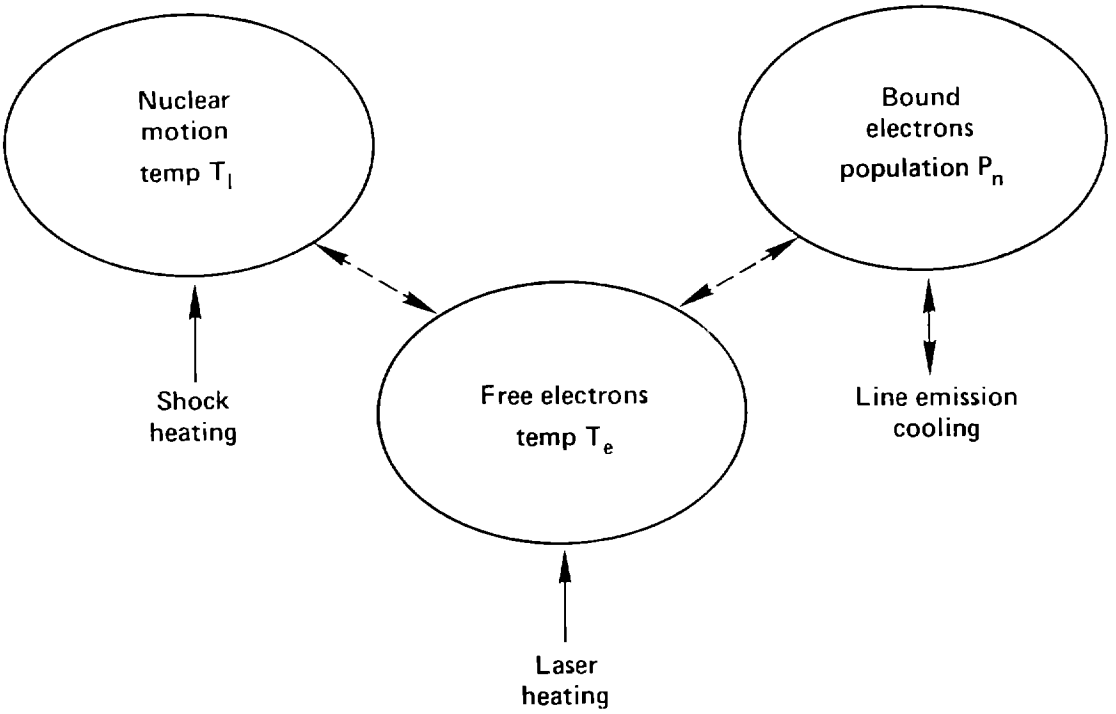

FIG. 22. Although nonequilibrium processes are relatively complicated, one achieves some degree of understanding by concentrating upon the dominant flow of thermal energy.

screened hydrogenic energies, uncorrected hydrogenic oscillator-strengths and omitting dielectronic recombination and autoionization rates. Nevertheless the strong effect of NLTE ionization cannot be missed. Without NLTE computational capability one cannot realistically describe high-Z laser interactions.

Lower-Z targets are often fully-ionized in the laser interaction region and the question of non-LTE becomes moot.

In short-wavelength irradiation one would expect reduced NLTE effects for several reasons: first, the laser absorption now occurs mainly by inverse bremsstrahlung which does not produce energetic suprathermal electrons; second, the absorption occurs at higher densities where the collisional rates are large enough to pull atomic populations toward LTE; third, the higher density also implies greater optical depth and a stronger radiation field which also brings the atoms closer to equilibrium.

Experiments on Be, CH, Ti and Au disks at shorter wavelength (λ = .53 μ) are analyzed by Mead et al.[100] These authors conclude that use of a NLTE model remains essential for mid- to high-Z targets, and large errors would be made in ionization and coronal temperatures if LTE were artificially enforced in the calculation.

Because of the complexity of the nonequilibrium processes we offer only one simple generalization which helps to interpret or guess the role of nonequilibrium in laser plasma hydrodynamics:

G-12.) Steady-state nonequilibrium plasmas can be described with heat-bath pictures which exhibit the mechanism and direction of energy flow.

In a steady ablation plasma, energy is absorbed via laser heating of the free electrons and then converted to radiation and ion expansion flow. Because up to 50 % of the absorbed energy is emitted as recombination and line radiation, one can say that this energy flows through or is processed by the bound electrons.

The bound electrons function as a thermodynamic subsystem (heat bath) collisionally coupled to a hotter bath of free electrons and radiatively coupled to the colder photon field. For optically thin plasmas most photons escape and the ambient radiation field is low, corresponding to a zero-temperature bath or heat sink.

According to LASNEX plasma simulations, the non-LTE ionization in laser plasmas is intermediate between a coronal equilibrium, corresponding to zero photon temperature, and LTE per se.

At these conditions the bound populations are described by an intermediate temperature determined by the relative strength of collisional and radiative couplings.

For heavy atoms the radiative rates (scaling with Q^4) become very large, as do the optical depths. In high-Z disk

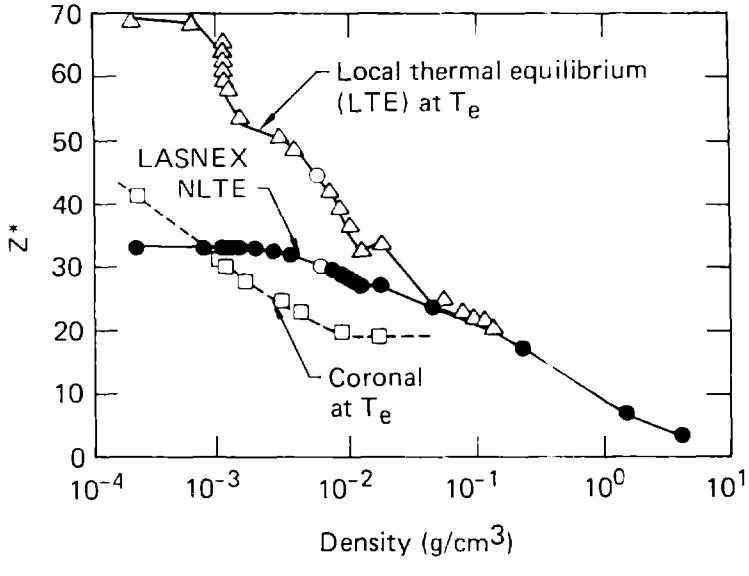

FIG. 23. LASNEX calculations of ionization for a planar-target ablation plasma (Z = 79). The NLTE charge state is significantly different from LTE or coronal models using the local free-electron temperature.

experiments one finds bound populations and even ion charge states effectively determined by the photon field which itself is cooler than the electron distribution.

These statements broadly characterise nonequilibrium target calculations. In typical ablation plasmas we do not find evidence of transient NLTE until relatively low densities are reached, at which point the charge state is frozen. At the higher densities a steady-state picture is adequate.

Reference 3 describes a quantitative development of these ideas: for plasmas with $|T_R - T_e| \ll T_e$, the NLTE steady-state is characterized by the principle of minimum entropy production, which roughly translates into a statement that the atomic populations adjust themselves to minimize the efficiency of conversion of electron thermal energy to x-rays.

Figure 21 indicates an entirely different heat-bath picture for nonequilibrium plasmas, in which electron and ion systems are coupled by slow energy exchange. During most of the laser-target interaction the ion temperature is predicted to lag behind the electron temperature by as much as 50 %. This form of nonequilibrium has less effect on the overall plasma dynamics, but the ion temperature plays a role in setting the Coulomb logarithm which enters the laser absorption, affects ion Doppler broadening, and of course enters into thermonuclear reaction rates.

These remarks underline the importance of nonequilibrium phenomena in laser-produced plasmas. The reader will find further information in specialized review articles on non-LTE atomic physics (McWhirter[101]), spectroscopic diagnostics (deMichelis and Mattioli,[102] Peacock, and Griem[103]), line formation and transport (Mihalas,[26] Kunasz[104]) and x-ray laser physics (Hagelstein,[37] Pert,[105] Jaegle[106]).

APPENDIX

A. Saha Problems

For hydrogen plasmas the Saha equation reduces to a simple (quadratic) form. Assume

n_o = number/cm^3 of neutral hydrogen atoms

n_+ = number/cm^3 of positive ions (protons)

$n_i = n_o + n_+$ = total atomic density

Because the plasma is neutral, the electron number density is $n_e = n_+$. The Saha equation is then

$$\frac{n_e n_+}{n_o} = \frac{2}{\lambda^3} \frac{1}{G_N} \exp\left(-\frac{I_o}{kT}\right) \qquad \text{(A-1)}$$

where $\lambda = (2\pi\hbar^2 / mkT)^{1/2}$

= electron thermal deBroglie wavelength

$I_o = e^2/2a_o$ = 13.6 eV = ionization potential

$\epsilon_n = -I_o / n^2$ = electron energy for principal quantum number n

$G_N = \sum_{n=1}^{N} 2n^2 \, e^{-(\epsilon_n - \epsilon_1)/kT}$

= atomic partition function (N = maximum allowed quantum number)

The average ionization state is $Q = n_e/n_i = n_e/(n_o + n_+)$, and define

$$A \equiv \tfrac{1}{2} n_I \lambda^3 \, G_N(T) \exp(I_o / kT)$$

Eq. (A-1) is then

$$1 - Q = AQ^2 \quad \text{or} \quad Q = \frac{1}{2A}\left(\sqrt{1+4A} - 1\right) \qquad \text{(A-2)}$$

Example 1. Show that $\Gamma_{ei} = Qe^2 / R_o kT < .54$ for all ρ, T.

This result illustrates rule G-4 of the text. Γ_{ei} is the electron-ion coupling parameter defined in Eq. (41). The theorem is based on the Saha equation and fails at high-density/low-temperature conditions where the Saha equation where the Saha equation fails. The proof is very simple: one forms the quantity Γ_{ei}^3 and uses Eq. (12) and the definition of the deBroglie length λ to show:

$$\Gamma_{ei}^3 = \frac{n_i \lambda^3}{2} \left(\frac{8}{3\sqrt{\pi}}\right) Q^3 \left(\frac{I_o}{kT}\right)^{3/2}$$

The Saha equation is used to replace $n_i\lambda^3$, giving

$$\Gamma_{ei}^3 = \frac{Q(1-Q)}{G_N} \frac{8}{3\sqrt{\pi}} \left(\frac{I_o}{kT}\right)^{3/2} \exp\left(-\frac{I_o}{kT}\right) \qquad \text{(A-3)}$$

From this it can be seen that Γ_{ei}^3 never exceeds $0.154/G_N$, because

$$Q(1-Q) \leq 0.25 \text{ all } Q$$

$$x^{3/2}e^{-x} \leq 0.41 \text{ all } x \; .$$

No matter how one handles the truncation of excited states in G_N we expect $G_N > 1$ and the theorem follows.

Example 2. The Saha equation agrees with the average-atom model for strongly ionized plasmas but disagrees significantly for the nearly-neutral case.

The relative merits of average-atom and Saha theories are a perennial subject of discussion. For hydrogen we have exact analytic solutions which throw some light on the (rather subtle) difference of the two approaches.

Using the Saha equation, we form the average population $\langle P_n \rangle$ for the shell of principal quantum number n:

$$\langle P_n \rangle = 2n^2 \frac{e^{-(\epsilon_n - \epsilon_1) / kT}}{G_N} \frac{n_o}{n_i}$$

$$= 2n^2 \frac{Q}{e^{(\epsilon_n - \mu) / kT}} \qquad \text{(A-4)}$$

In the second form of this equation we employ the definition of the electron chemical potential μ appropriate to nondegenerate free electrons:

$$n_e = Q n_i = \frac{2}{\lambda^3} e^{\mu/kT} \qquad \text{(A-5)}$$

In the average-atom model, the shell populations are calculated by Fermi-Dirac statistics,

$$\bar{P}_n = \frac{2n^2}{1 + \exp(\frac{\epsilon_n - \mu}{kT})} \qquad \text{(A-6)}$$

In this equation the chemical potential μ is determined by the requirement of neutrality,

$$Q + \sum_n P_n = 1 \qquad \text{(A-7)}$$

For a given plasma density ($= n_i$) and temperature, the charge state Q and electron chemical potential μ of the two theories could differ.

Comparing Eqs. (A-4) and (A-6) strongly for ionized plasmas ($Q \simeq 1$) we see that the two theories predict essentially equal chemical potentials and equal (small) boundstate populations.

In the nearly neutral case ($Q \ll 1$) the situation is more interesting. For the Saha equation, this limit is achieved whenever $\exp((\epsilon_1 - \mu)/kT) \ll 1$; for the average-atom theory, the nearly-neutral case occurs only if $\mu \simeq \epsilon_1$. The resulting approximate forms are:

$$Q_{Saha} \simeq \frac{\exp(\epsilon_1/kT)}{n_i \lambda^3}^{1/2} \quad ; \quad Q_{AA} \simeq \frac{2}{n_i \lambda^3} e^{\epsilon_1/kT} \; .$$

Surprisingly these do not agree; instead

$$Q_{AA} \simeq 2 Q_{Saha}^2 \ll Q_{Saha} \qquad \text{(A-8)}$$

and in this limit the average-atom model predicts a much lower degree of ionization.

Further analysis of the equations reveals that this prediction is caused by an exaggerated binding energy for

negative ions in the average-atom theory. Of course, the "exact" Saha theory altogether ignored the possibility of negative ions.

Example 3. We consider a highly ionized hydrogen plasma in complete thermal equilibrium, containing only a small density of neutral atoms. We will show that the neutrals cannot dominate the stopping power for charged particles even though bound electrons are individually much more effective at absorbing energy transfers due to their lower velocities.

This calculation illustrates rule G-8. The assumptions are

$$v_o \ll v_{ion} \ll v_e \tag{A-9}$$

where $v_o = e^2 / \hbar$ = Bohr velocity, $v_e = \sqrt{kT/m}$ = free electron thermal velocity. With these assumptions the stopping power for an ion of charge Z_1, velocity v_{ion} is a sum of contributions from bound and free electrons,

$$\frac{dE}{dx} = \frac{4\pi Z_1^2 e^4}{m v_{ion}^2} \left[n_o \log\left(\frac{2mv_{ion}^2}{\bar{I}}\right) + a\, n_e \left(\frac{v_{ion}}{v_e}\right)^3 \log\left(\frac{2kT}{\hbar\omega_p}\right) \right] \tag{A-10}$$

where $a = (1/3)\sqrt{2/\pi}$ and $\bar{I} \sim 15$ eV is the hydrogen average ionization excitation potential. The question is whether the first term can ever be dominant as a consequence of the velocity ratio in the free electron term.

Using the Saha equation, the ratio of the two contributions can be expressed

$$\frac{(dE/dx)_{Bound}}{(dE/dx)_{Free}} = a_o^3 n_+ \left(\frac{V_o}{V_{ion}}\right)^3 (3\pi^2 G_N) L \tag{A-11}$$

where L = ratio of logarithms, $a_o = \hbar^2/2m$.

This ratio is small ($\ll 1$) except at high densities where $a_o^3 n_+ \simeq 1$ but in that case the K-shell is pressure ionized according to the ion-sphere criterion.

Note that $G_N \simeq 2N^3/3 \propto n_+^{-1/2}$ so the product $n_+ G_H$ does not become large at low densities.

ACKNOWLEDGEMENT

The author is grateful to Drs. D. A. Liberman, F. J. Rogers, and E. J. McGuire for providing numerical results quoted in the text.

Work performed under the auspices of the U.S. Department of Energy by the Lawrence Livermore National Laboratory under contract number W-7405-ENG-48.

REFERENCES

1. An excellent overview is given by the series Laser Program Annual Report, Lawrence Livermore National Laboratory, UCRL-50021 (1978 to the present).
2. R. M. More, Atomic Physics in Inertial Confinement Fusion, preprint UCRL-84991, Lawrence Livermore National Laboratory (1981).
3. R. M. More, Atomic and Molecular Physics of Controlled Thermonuclear Fusion, p. 399, Ed. by C. Joachain and D. Post, Plenum Publishing Corp. (1983).
4. Proceedings of Workshop Conference on Radiative Properties of Hot Dense Plasmas, J.Q.S.R.T. 27, p. 209-385 (1982); Radiative Properties of Hot Dense Matter, Ed. by J. Davis, C. Hooper, R. Lee, A. Merts, and B. Rozsnyai, World Scientific, Singapore (1985).
5. M. J. Herbst, P. G. Burkhalter, D. Duston, M. Emery, J. Gardner, J. Grun, S. P. Obenschain, B. H. Ripin, R. R. Whitlock, J. P. Apruzese and J. Davis, Laser Interaction and Related Plasma Phenomena, Vol. 6, Ed. by H. Hora and G. Miley, p. 317, Plenum Press, New York (1984).
6. Dr. J.-C. Gauthier et al., unpublished paper presented at this meeting.
7. M. D. Rosen, P. L. Hagelstein, et al., Phys. Rev. Lett. 54, 106 (1985); D. L. Matthews, P. L. Hagelstein, et al., Phys. Rev. Lett. 54, 110 (1985).
8. E. A. Crawford and A. L. Hoffman, in Laser Interaction and Related Plasma Phenomena, Vol. 6, p. 353, Ed. by H. Hora and G. Miley, Plenum Press, New York (1984).
9. R. M. More, in Laser Interaction and Related Plasma Phenomena, Vol. 5, p. 253, Ed. by H. J. Schwarz, H. Hora, M. J. Lubin and B. Yaakobi, Plenum Press, New York (1981).
10. D. K. Bradley, J. Hares, A. Rankin and S. J. Rose, The analysis of colliding-shock experiments, Rutherford Appleton Laboratory, preprint RAL-85-020, (1985).
11. A. Ng, D. Parfeniuk, P. Celliers, L. DaSilva, University of British Columbia, Vancouver B.C., preprint "Electrical Conductivity of a Dense Plasma" (Nov. 1985).
12. R. Fabbro, B. Faral, J. Virmont, F. Cottet, J. P. Romain and H. Pepin, Phys. Fluids 28, 3414 (1985).
13. Ya. B. Zel'dovich and Yu. P. Raizer, Physics of Shock Waves and High-Temperature Hydrodynamic Phenomena, Vol. 1, Ed. W. D. Hayes and R. F. Probstein, Academic Press, New York (1966).
14. B. Strömgren, Zs. f. Ap. 4, 118 (1932).
15. H. Mayer, Los Alamos Scientific Laboratory report LA-647 (unpublished) 1947.
16. W. Lokke and W. Grasberger, Lawrence Livermore Laboratory report UCRL-52276 (1977).
17. G. B. Zimmerman and R. M. More, J.Q.S.R.T. 23, 517 (1980).
18. R. M. More, J.Q.S.R.T. 27, 345 (1982).
19. A. Sommerfeld, Atomic Structure and Spectral Lines, 3rd Ed. Methuen, London (1934).
20. D. Salzmann and G. Wendin, Phys. Rev. A18, 2695 (1978).

21. V. C. Reddish, Physics of Stellar Interiors, Edinburgh University Press, Edinburgh (1974).
22. R. M. More, Advances in Atomic and Molecular Physics, 21, 305 (1985). We note that the usual discussion concerns line shifts (not level shifts).
23. L. Spitzer, Jr., Physics of Fully Ionized Gases, 2nd Rev. Ed., Interscience Publishers, New York (1962).
24. E. E. Salpeter, J. Geophysical Research 68, 1321 (1963).
25. G. Ecker, Z. fur Phys. 148, 593 (1957).
26. D. Mihalas, Stellar Atmospheres, 2nd Ed., W. H. Freeman & Co., San Francisco, p. 294 (1978).
27. R. Dicke, Phys. Rev. 89, 472 (1953).
28. D. Burgess, D. Everett and R. Lee, J. Phys. B-12, L755 (1979).
29. J. Green, J.Q.S.R.T. 4, 639 (1964).
30. S. Brush, H. Sahlin and E. Teller, J. Chem. Phys. 45, 2102 (1966).
31. J.-P. Hansen, Phys. Rev. A8, 3096 (1973).
32. M. Baus and J.-P. Hansen, Physics Reports 59, 1 (1980).
33. H. E. DeWitt, Strongly Coupled Plasmas, p. 81, Ed. by G. Kalman and P. Carini, Plenum Publishing Corp. (1978).
34. R. W. Hockney and J. W. Eastwood, Computer Simulation Using Particles, McGraw-Hill, New York (1981).
35. R. B. Laughlin, Lawrence Livermore National Laboratory, Livermore, CA, preprint UCRL-90304, to appear in Physical Review A.
36. R. M. More, in Laser Program Annual Report, UCRL-50021-84, p. 3-68, Lawrence Livermore National Laboratory, Livermore, CA (1984).
37. P. Hagelstein, Physics of Short Wavelength Laser Design, Lawrence Livermore National Laboratory, Livermore, CA, UCRL-53100 (1981).
38. L. D. Landau, JETP 7, 203 (1937). The careful reader will observe there is a numerical mistake in the final result of this paper.
39. C. C. Klick and J. H. Schulman, Solid State Physics 5, 97 (1957);
D. Dexter and R. Knox, Excitons (Interscience, New York, NY, 1965).
40. G. Ecker and W. Kröll, Physics of Fluids 8, 354 (1965).
41. D. A. Liberman, Phys. Rev. B20, 4981 (1979);
D. A. Liberman, J.Q.S.R.T. 27, 335 (1982).
42. F. Perrot, Phys. Rev. A26, 1035 (1982).
43. R. Cauble, M. Blaha and J. Davis, Phys. Rev. A29, 3280 (1984).
44. R. M. More, Advances in Atomic and Molecular Physics, 21, 305, (1985).
45. D. Burgess, unpublished report CLM-P 567, Culham Laboratory, Abingdon, UK (1978).
46. N. J. Peacock, unpublished report CLM-P 519, Culham Laboratory, Abingdon, UK (1977).
47. S. Brush and B. H. Armstrong, Proceedings of Workshop Conference on Lowering of the Ionization Potential, JILA report 79, Univ. of Colorado, Boulder, CO (1965).
48. A. Unsold, Z. Astrophys. 24, 355 (1948).
49. T. Carson and H. Hollingsworth, Mon. Not. R. Astron. Soc. 141, 77 (1968);
T. Carson, D. Mayers and D. Stibbs, Mon. Not. R. Astron. Soc. 140, 483 (1968).

50. D. Burgess and R. L. Lee, Journal de Physique 43, Colloque C2, 413, (1982).
51. F. J. Rogers, H. C. Graboske, H. DeWitt, Physics Letters 34A, 127 (1971).
52. J. Weisheit and B. Shore, Astrophys. J., 194, 519 (1974).
53. A. Vinogradov, I. Sobelman, and E. Yukov, Sov. J. Quantum Electron. 4, 149 (1974).
54. S. Brush, H. Sahlin and E. Teller, J. Chem. Phys. 45, 2102 (1966).
55. F. J. Rogers, unpublished preprint.
56. H. R. Griem, Plasma Spectroscopy, McGraw-Hill, New York (1964).
57. J. Stewart and K. Pyatt, Astrophys. J. 144, 1203 (1966).
58. J. Humblet, Mem. Soc. R. Sci. Liege 12, 9 (1952); B. Ya. Zel'dovich, Soviet Physics JETP 12, 542 (1961); R. M. More, Phys. Rev. A 4, 1782 (1971).
59. T. Regge, Nuevo Cimento VIII, 671 (1958).
60. C. Bauche-Arnoult, J. Bauche, and M. Klapisch, Phys. Rev. A 20, 2424 (1979); 25, 2641 (1982); M. Klapisch, E. Meroz, P. Mandelbaum, A. Zigler, C. Bauche-Arnoult, and J. Bauche, ibid. 25, 2391 (1982). C. Bauche-Arnoult, J. Bauche, and M. Klapisch, Phys. Rev. A 31, 2248 (1985).
61. P. Audebert, J.-C. Gauthier, J.-P. Geindre, and C. Chenais-Popovics, C. Bauche-Arnoult, J. Bauche, M. Klapisch, E. Luc-Koenig, and J.-F. Wyart, Phys. Rev. A32, 409 (1985).
62. J. M. Green, J.Q.S.R.T. 19, 639 (1964).
63. F. Grimaldi and A. Grimaldi-Lecourt, J.Q.S.R.T. 27, 373 (1982).
64. M. Busquet, D. Pain, J. Bauche, and E. Luc-Koenig, Physica Scripta 31, 137 (1985).
65. D. Duston and J. Davis, Phys. Rev. A21, 1664 (1980). Figure 3 of this paper illustrates the (incorrect) recombination predicted by rate equations at high densities.
66. J. Scott, Philos. Mag. 43, 859 (1952); J. Schwinger, Phys. Rev. A22, 1827 (1980).
67. F. J. Rogers, Phys. Rev. A24, 1531 (1981).
68. This equation for the density matrix of a one-electron system is easily derived from the definition given.
69. A. Dalgarno, lectures presented at this meeting.
70. R. M. More, Lawrence Livermore National Laboratory report UCRL-84379, Two-Temperature Equation of State for Dense Plasmas (1980); D. A. Boercker and R. M. More, Phys. Rev. A, to be published.
71. B. J. B. Crowley and R. M. More, Proceedings of Workshop Conference on Atomic Physics for Heavy-Ion Fusion, Rutherford-Appleton Laboratory, October, 1984.
72. J. D. Jackson, Classical Electrodynamics, 2nd Ed., J. Wiley & Sons, Inc., New York, p. 724 (1975).
73. S. Skupsky, Phys. Rev. A16, 727 (1977).
74. International Workshop on Atomic Physics for Ion Driven Fusion, Journal de Physique, Colloque No. 8, Tome 44, Suppl. an FASC.II (1983); C. Deutsch, G. Maynard and H. Minoo, Journal de Physique C8, 67 (1983).
75. J. A. Harte and R. M. More, Lawrence Livermore National Laboratory, unpublished report UCRL-50021-82, "Laser

Program Annual Report," p. 3-66.
76. E. J. McGuire, PRA26, 125 (1982); E. J. McGuire, J. M. Peek and L. C. Pitchford, Phys. Rev. A26, 1318 (1982).
77. M. J. Seaton, Comptes Rendus 240, 1317 (1955); N. F. Mott and H. S. W. Massey, Theory of Atomic Collisions, 3rd Ed., p. 68, Oxford Univ. Press, London (1965).
78. R. Peierls, Surprises in Theoretical Physics, p. 137, Princeton Univ. Press, Princeton, N.J., 1979.
79. A. Burgess, Ap. J. 139, 776 (1964); A. Burgess, Ap. J. 141, 1588 (1965); A. Burgess and A. S. Tworkowski, Ap. J. 205, L-105 (1976); A. Merts, R. D. Cowan, and N. H. Magee, Jr., unpublished report LA-6220-MS (1976).
80. H. A. Kramers, Philos. Mag. 271, 836 (1923).
81. L. D. Landau and E. M. Lifshitz, Classical Theory of Fields, 2nd Ed., Pergamon Press, Oxford, 1962.
82. W. J. Karzas and R. Latter, Astrophysical Journal Suppl. no. 55, Vol. VI, p. 167 (1961); P. J. Brussard and H. C. Van de Hulst, Rev. Mod. Phys., 34, 507 (1962); I. P. Grant, Mon. Not. R. Astron. Soc. 118, 352 (1958).
83. M. Lamoureux and R. H. Pratt, Radiative Properties of Hot Dense Matter, p. 241, Ed. by J. Davis et al., World Scientific, Singapore (1985).
84. V. I. Kogan and A. B. Kukushkin, Soviet Physics JETP 60, 665 (1984).
85. J. J. Feng and R. H. Pratt, unpublished preprint.
86. C. M. Lee and R. H. Pratt, Phys. Rev. A12, 707 (1975).
87. J. P. Cox and R. T. Giuli, Principles of Stellar Structure, Vol. 1, Gordon and Breach, New York, 1968.
88. J. Dawson and C. Oberman, Physics of Fluids 6, 394 (1963).
89. B. F. Rozsnyai, J.Q.S.R.T. 22, 337 (1979).
90. J. M. Green, R. and D. Associates unpublished report RDA-TR-108600-003 (1980).
91. M. Lamoureux, I. J. Feng, R. H. Pratt and H. K. Tseng, J.Q.S.R.T. 27, 227 (1982).
92. L. Kim, R. H. Pratt and H. K. Tseng, Phys. Rev. A32, 1693 (1985).
93. S. Ichimaru, Basic Principles of Plasma Physics, W. A. Benjamin, Inc., Reading, Mass. 1973.
94. M. Lamoureux, C. Möller and P. Jaegle, Phys. Rev. A30, 429 (1984).
95. W. Huebner, M. F. Argo and L. D. Ohlsen, J.Q.S.R.T. 19, 93 (1978).
96. H. A. Bethe and E. E. Salpeter, Quantum Mechanics of One- and Two-Electron Atoms, Academic Press, Inc., New York, 1957.
97. S. J. Rose, Rutherford-Appleton Laboratory, unpublished preprint RL-82-114, "The Effect of Relativity on the Oscillator Strengths of Hydrogen-Like Ions," Dec. 1982.
98. O. Benka and R. Watson, Phys. Rev. A29, 2255 (1984).
99. M. D. Rosen, D. W. Phillion, V. C. Rupert et al., Phys. Fluids 22, 2020 (1979).
100. W. C. Mead, E. M. Campbell et al., Phys. Fluids 26, 2316 (1983).
101. R. W. P. McWhirter in Plasma Diagnostic Techniques, ed. by R. Huddlestone and S. Leonard, Academic Press,

New York, 1965.
102. C. DeMichelis and M. Mattioli, Rep. Prog. Phys. 47, 1233 (1984).
103. H. R. Griem, Handbook of Plasma Physics, eds. M. N. Rosenbluth and R. Z. Sagdeev, Vol. 1, p. 73, North-Holland, 1983.
104. P. Kunasz, in Radiative Properties of Hot Dense Matter, ed. by J. Davis, C. Hooper, R. Lee, A. Merts, B. Rozsnyai, p. 3, World Scientific, Singapore, 1985.
105. G. J. Pert, preprint, University of Hull, "SUV and X-ray Lasers," to be published.
106. P. Jaegle, lectures presented at this meeting.